Optimization of Power Cable Production Lines for EPM/EPDM Elastomers by Genetic Algorithm with Different Peroxides

G. Milani,[1] F. Milani[2]

[1]*Institute of Structural Engineering (IBK), Swiss Federal Institute of Technology (ETHZ), Wolfgang Pauli Strasse 15, Zürich 8093, Switzerland*
[2]*CHEM.CO, Via J.F.Kennedy 2, Occhiobello, Rovigo 45030, Italy*

Received 6 September 2007; accepted 21 June 2008
DOI 10.1002/app.29087
Published online 9 October 2008 in Wiley InterScience (www.interscience.wiley.com).

ABSTRACT: EPM/EPDM elastomers are widely used for the insulation of high and medium voltage electric cables. Insulator mechanical properties depend on the extent of vulcanization, which is obtained by manufactures using a number of different peroxides as cross-linking agents. Vulcanization occurs in the continuous vulcanization tube, a pressurized tube filled with nitrogen at high temperatures. Then, water and/or air are used to cool the cable at ambient temperature. Changes of process variables cause considerable changes in insulator physical properties. In the present article, a genetic algorithm with zooming and elitist strategy is used for the determination of optimal production lines parameters to use to maximize rubber output mechanical properties. Nitrogen temperature T_s and exposition time t are assumed as production parameters to optimize, whereas two different output mechanical properties (tensile strength and tear resistance) are considered as objective functions. Several optimization problems are analyzed both for medium and high voltage cables. A final multiobjective optimization is presented with the corresponding Pareto frontier, where objective functions are represented by tear resistance and tensile strength. Optimal production T_s and t are obtained for all the cases analyzed. Numerical simulations show how different peroxides and insulator thicknesses sensibly influence optimal production variables. © 2008 Wiley Periodicals, Inc. J Appl Polym Sci 111: 482–507, 2009

Key words: calculations; EPM/EPDM elastomers; vulcanization; genetic algorithm; insulation of electric cables

INTRODUCTION

The vulcanization process in continuum of wires and cables has been in industrial practice for nearly 50 years. Therefore, the study of the mechanical performance of polymers and copolymers used as insulators is of great technical interest. At present, industrial processes of insulation of medium and high voltage cables utilize almost only polyethylene (PE) and ethylene propylene copolymers (EPM/EPDM), even with the utilization of polybutadiene resins as coagents.[1,2]

Among the others, the following concurring reasons lead manufactures to prefer PE and EPM/EPDM elastomers: (1) their good dielectrical strength, which is the ability to withstand electrical stress under standard and emergency conditions; (2) their life expectation, evaluated by means of the first derivative of the electric life curve, representing the ageing rate when long time performance under electrical stress is considered; (3) their resistance to partial discharges (i.e., their ability to maintain original properties under ionization caused by voids or other faults, which act as additional ageing factors); (4) their permectivity and dissipation factors, which strongly influence the amount of dielectric losses in the insulation layer; (5) their resistance to water penetration. On the other hand, the needs of producers vary considerably, according to both the specific products that they intend to obtain and the physical limitations within they must work (i.e., economical and production constraints, intended as temperature work ranges, production line lengths and velocity range, etc.). In the production processes, it should be preferred the utilization of EPM/EPDM elastomers instead of PE for high and medium/high voltage cables, due to a number of advantages which can be obtained with EPM/EPDM, as for instance the possibility to avoid the so called electrical treeing[3] and the possibility to mix peroxides and EPM/EPDM rubber during the preprocessing phase at lower temperatures with respect to PE. This allows, for instance, the use of a wide spread of commercial peroxides, as well as it ensures a defined level of vulcanization of the final product. On the other hand, level of vulcanization is a key aspect for the determination of final mechanical properties of the

Correspondence to: G. Milani (gmilani@ing.unife.it or milani@ibk.baug.ethz.ch).

insulator. Thus, it appears clear that it could be particularly useful from a practical point of view to have an idea of the most appropriate production parameters to use to enhance resultant insulated cables.

In industrial practice, the hot elastomers are applied to the conductor by extrusion. The coated cable passes through the so-called continuous vulcanization tube (CV), a pressurized tube filled with nitrogen at high temperatures at which the cross-linking agent is highly active. Then, water and/or air are used to cool the insulated cable at ambient temperature. As well know, the most important phase of all the production line is the vulcanization tube, where rubber assumes its final mechanical properties. Therefore, changes of process variables associated with the CV tube can cause considerable changes in insulator physical properties, ageing characteristics and heat resistance.

In this framework, in the present article, a metaheuristic model (genetic algorithm, GA) devoted to the optimization of medium and high voltage cables production lines cross-linked with ethylene-propylene copolymers is presented.

A mathematical model is adopted to describe the dry cured vulcanization line with EPM/EPDM. The insulation material is regarded as constituted by a number of layers disposed with cylindrical symmetry with respect to the cable axis, each one withstanding different temperatures at different times during the production process. The well known Fourier's law of heat transmission is used both for the insulator material and the conductor with the aim of obtaining temperature profiles for each insulator layer at each time step. In this way, a partial differential equation system (PDES), solved by means of finite differences methods, is obtained.

Once that temperature profiles are at disposal for each layer, optimization of the production process is obtained by means of the GA proposed, assuming as objective functions mechanical properties (e.g., tensile strength and tear strength) of the vulcanized rubber.

Input variables (i.e., production line parameters to optimize) are represented by nitrogen temperature T_s and exposition time t (closely related to production line speed). Obviously, a number of other production variables could be considered; nevertheless, experimental evidences show that the aforementioned input parameters are particularly important, since they influence insulator output mechanical properties in a considerable way, being directly connected to curing time and layers temperature profile.

On the other hand, rubber tensile strength and tear resistance are monitored as quantities to optimize. Despite the fact that only these two outputs are considered in the article, the approach proposed is aimed at selecting any output mechanical property as optimization objective function, meaning that the procedure could be used by manufactures in a general framework. In this context, it is worth noting that a key aspect that makes the optimization of power cables lines a very complex task, is the relation among half life of peroxides used ($t_{1/2}$), representing the time at which $1/2$ of the initial moles of the peroxide in the mixture has reacted, temperature of each layer of the insulator during the heating process and mechanical properties of rubber as a function of unreacted peroxide.

In particular, several questions arise from the previous aspects, related to the fact that experimental evidences[4–8] show that rubber inelastic mechanical properties (e.g., tensile strength, tear resistance) depend nonmonothonically on the curing time via unreacted peroxide concentration C_i. In particular, for high values of C_i, rubber results not vulcanized with a very low tensile/tear strength, whereas for lower values of C_i, experience shows that an optimal concentration $\overline{C}_i$ exists where output mechanical properties reach their maximum. Usually, such concentration is not the same for both tear and tensile strength,[4–6,9] leading to a nontrivial multiobjective optimization problem.[10] In this latter case, Pareto optimality frontiers[11–14] must be recovered, to have practical information on the input variables to prefer. On the other hand, peroxide half life $t_{1/2}$ results strongly dependent on exposition temperature. Obviously, each insulator layer undergoes different temperature histories during the production process, meaning that the peroxide reaction velocity varies for each layer at different time steps in a different way.

Peroxide reaction velocity for each layer is monitored numerically with the aim of maximizing output objective functions selected. Maximization is obtained by means of a novel GA approach based on a specifically crafted zooming strategy, consisting in the subdivision of the population at each iteration into two subgroups, depending on individuals grade of fitness (elitist strategy). Different genetic procedures are applied to the subgroups, consisting of both two typologies of admissible mutations for the elite subpopulation and mutation and reproduction for the remaining individuals. In order to improve algorithm convergence, a user-defined population percentage, depending on individuals fitness, is replaced with new phenotypes at the end of each iteration, enforcing in this way the chromosomes renewal.

POWER CABLES PRODUCTION LINES

The industrial process of cross-linking of power cables is usually obtained by means of horizontal (catenary continuous vulcanization CCV) or vertical

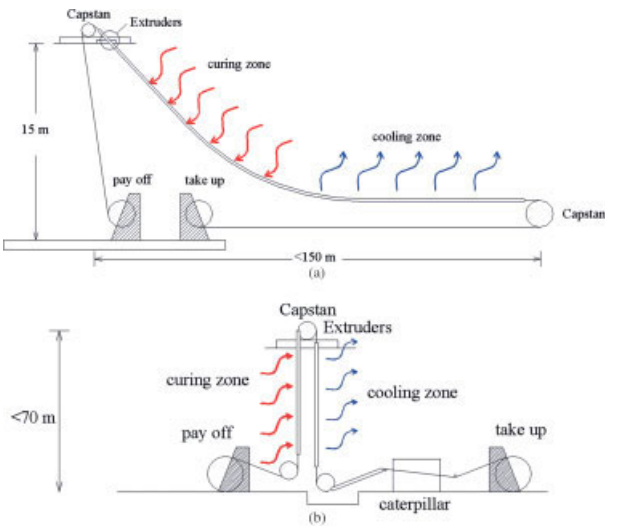

Figure 1 Industrial process of cross-linking of power cables. (a) horizontal (b) vertical. [Color figure can be viewed in the online issue, which is available at www.interscience.wiley.com.]

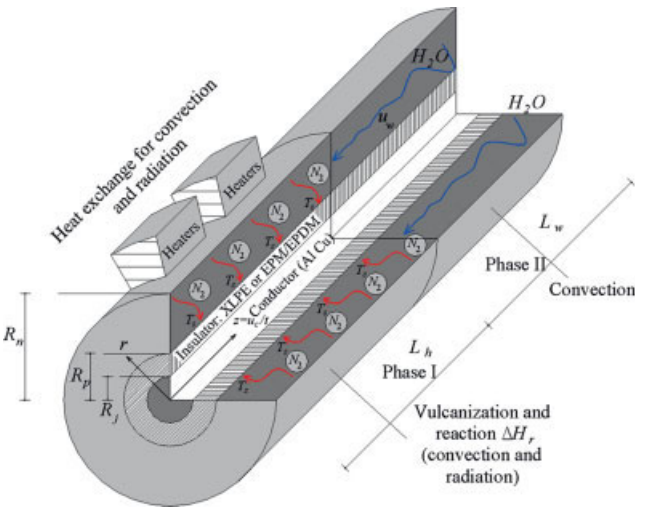

Figure 2 Schematic representation of heating phase (Phase I) and cooling phase (Phase II) with water. [Color figure can be viewed in the online issue, which is available at www.interscience.wiley.com.]

production lines (vertical continuous vulcanization VCV), see Figure 1.

In both cases, a heating zone is followed by a cooling phase with water and/or air. In the first phase, cross-linking of polymer is obtained by dry curing under high pressure in a tube filled with nitrogen. Process starts in an extruder (1), where the conductor (Al or Cu) is coated with the extruded EPM/EPDM. Then the cable enters the heating zone (2), filled with nitrogen at high pressure and high temperature. Finally, the cable is cooled to the ambient temperature in two steps: in the first step (3), cold water at around 10 bar pressure is used, finally the cable is leaved and cooled in the surrounding air by free convection (4). During the continuous process, in the curing tube the heat is transferred by convection and radiation from the tube wall through nitrogen to the cable surface, whereas in the cooling zone with water only convection plays an important role,[15–17] see Figure 2.

The vulcanization tube length for CCV lines can be up to 150 m (usually 60–80 m). Medium and high voltage cables have a diameter of 20–80 mm, with insulator thickness variable from 5 to 20 mm. For instance, Italian railways specifications[18] for subsuppliers of EPM/EPDM medium and high voltage cables used in the railways industry require cables diameters of 16.1 and 16–38.4 mm and insulators thicknesses of 5.5 and 10.8–20 mm for medium and high voltage cables respectively (see Table I).

To optimize the production line, many parameters have to be chosen carefully. In particular, the following variables play a crucial role: exposition time, temperature of the heated part of the tube filled with nitrogen, temperature and flow rate of the cooling water. From a practical point of view, exposition time is controlled by the production line speed, once that the vulcanization tube length is fixed. Usually, production plants have a vulcanization length which is difficultly changeable, being closely related to initial design specifications. Therefore, engineers can act only on cable velocity to modify exposition time.

Manufacturers select the aforementioned variables values on their own, usually following their experience on this field. Therefore, it appears particularly attractive from both a theoretical and practical point of view to purpose an optimization approach based on a Genetic Algorithm (GA) to use instead of experience, to confirm and/or improve manufacturers choices.

VULCANIZATION PROCESS BY PEROXIDIC RETICULATION

A number of different elastomers can be cross-linked using peroxides.[5,6,16,19,20]

When dealing with EPM/EPDM elastomers, cross-linking occurs by means of common organic

TABLE I
Medium and High Voltage Cables Conductor and Insulator Diameters (Data from Italian Railways Specifications)

	Conductor diameter [mm]	Insulator thickness [mm]	External PVC layer thickness [mm]
Medium voltage cables	16.1	5.5	2.5
High voltage cables	16–38.4	10.8–20	2.4–4

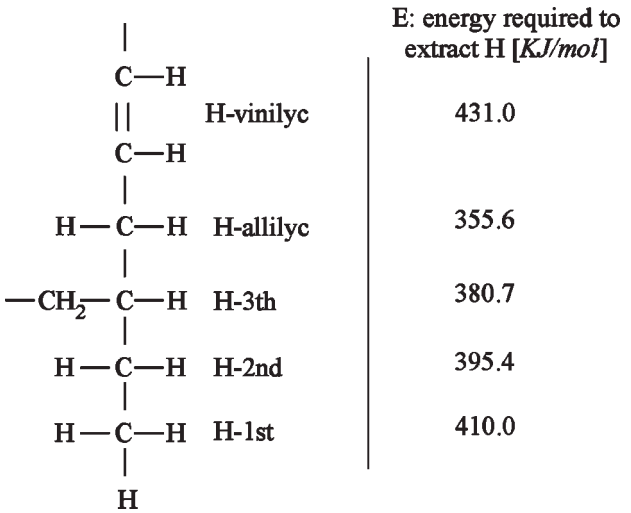

Figure 3 Energy required to extract hydrogen atom from the backbone of the macromolecules.

peroxides. EPM/EPDM rubber, in fact, is constituted by saturated linear macromolecules with a paraffinic structure, with controlled quantities of insaturations (for EPDM), external to the main chain.

At present, three of the most diffused cross-linking agents used in practice are $\alpha - \alpha'$-bis-(t-butylperoxy)-diisopropylbenzene, di-cumyl peroxide, and 1.1 bis(t-butyl-peroxy)-3.3.5 trimetylcyclohexane. From a practical point of view, passing from the first to the last peroxide, producers can increase curing rate at a fixed vulcanization temperature.

From a theoretical point of view, the selection of the most appropriate peroxide is a very difficult task since it is obviously necessary to have a deep knowledge of both the application to which the peroxide is used and the process method, as well as the operating conditions to be used.

The reaction temperature (which is a function of nitrogen temperature via partial differential equations) is the fundamental parameter on which the choice of the organic peroxide depends.

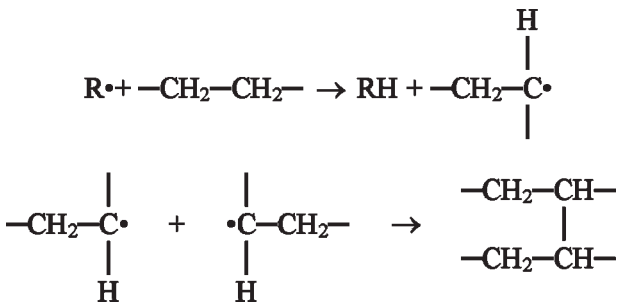

Figure 4 Peroxidic vulcanization of saturated hydrocarbon elastomers.

Vulcanization of saturated hydrocarbons elastomers through peroxides: general reticulation kinetics

The first step in a peroxide-induced vulcanization is the decomposition of the peroxide to give free radicals,[21,22] i.e., peroxide $\rightarrow 2R^{\bullet}$, where $R^{\bullet}$ is an alkoxil, an alkyl or an acyloxyl radical, depending on the typology of peroxide used.

As well known, the efficiency of the cross-linking process depends either on the difficulty (in an energetic meaning) to extract the hydrogen atom from the backbone of the macromolecules (see Baldwin and Ver Strate[21]), as shown in Figure 3. In the case of saturated hydrocarbon polymers,[23,24] see Figure 4, the efficiency is reduced by branching. In particular, using EPM/EPDM rubbers it has been shown that the efficiency is a function of the propylene content (Fig. 5 and Refs. 24–26). Therefore, a key aspect in the cross-linking process of EPM/EPDM rubber[27] is to have at disposal formulas to use in practice able to predict kinetic decomposition of peroxides as a function of rubber composition, vulcanization conditions (temperature and exposition time) and peroxide unreacted concentration.

As a rule, peroxides decomposition kinetic is of first order, meaning that its mathematical representation is a separable differential equation $-\frac{dC}{dt} = kC$, where C is the concentration (expressed for instance in mol/m^3) of the unreacted peroxide and k is a

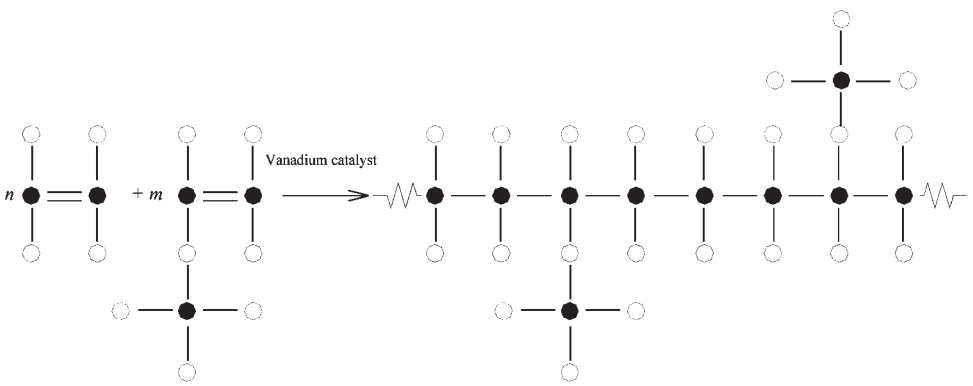

Figure 5 Basic structure of ethylene propylene copolymers.

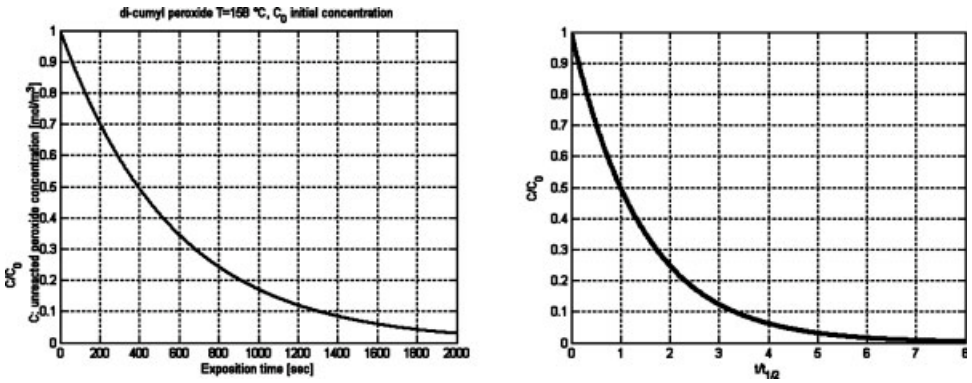

Figure 6 Peroxide decomposition time law at a fixed temperature (di-cumyl peroxide) and nondimensional $t/t_{1/2}-C/C_0$ curve (Akzo chemie data).

kinetic constant for a fixed peroxide. Its analytical solution can be obtained splitting variables, i.e.,

$$\int_{C_0}^{C(t)} \frac{dC}{C} = -\int_0^t k dt \Rightarrow \ln\left(\frac{C(t)}{C_0}\right) = -kt \Rightarrow C(t)/C_0 = e^{-kt} \quad (1)$$

where C_0 is the initial peroxide concentration (all unreacted) and $C(t)$ is the unreacted peroxide concentration at time t. Defining as half life $t_{1/2}$ the time required to obtained a concentration of unreacted peroxide equal to $C_0/2$, eq. (1) can be rewritten as follows:

$$\begin{aligned} 1/2 &= e^{-kt_{1/2}} \\ \Rightarrow k &= \ln 2/t_{1/2} \end{aligned} \quad (2)$$

Equation (2) permits to numerically obtain constant k once that parameter $t_{1/2}$ is known.

Therefore, from eq. (2), reaction kinetic law (1) can be rewritten as follows (see also Fig. 6):

$$\frac{C(t)}{C_0} = e^{-\frac{\ln 2}{t_{1/2}(T)}t} = e^{-\frac{\ln 2}{t_{1/2}(T)}t + \ln 2 - \ln 2} = e^{-\ln 2} e^{\left(1-\frac{t}{t_{1/2}(T)}\right)\ln 2} = \frac{1}{2} e^{\left(1-\frac{t}{t_{1/2}(T)}\right)\ln 2} \quad (3)$$

Equation (3) describes the absolute decrease of peroxide unreacted concentration at different times with respect to parameter $t_{1/2}$.

As experimental evidences show, the rate of reaction, hence $t_{1/2}$ (or analogously velocity constant k), are temperature dependent. In Figure 7, for instance, the behavior at different temperatures in terms of $t_{1/2}$ parameter for 32 different peroxides commonly used is reported. As well known, such a dependence is expressed by the classical Arrhenius equation[28,20]:

$$k(T) = k_{\max} e^{-\frac{E_a}{R_g T}} \quad (4)$$

where $k(T)$ is the peroxide velocity constant at a temperature T, E_a is the so-called energy of activation $\left[\frac{\text{kJ}}{\text{mol}}\right]$, R_g is the general gas constant ($8.134\left[\frac{\text{J}}{\text{mol K}}\right]$), T is the absolute temperature, $k_{\max}$ is the velocity constant for $T \to +\infty$.

Form eq. (4) and using eq. (2), it can be proved that:

$$t_{1/2}(T_2)/t_{1/2}(T_1) = e^{-\frac{E_a}{R_g}\left(\frac{1}{T_1}-\frac{1}{T_2}\right)} \Rightarrow \ln\left(t_{1/2}(T_2)\right) - \ln\left(t_{1/2}(T_1)\right) = \frac{E_a}{R_g}\left(\frac{1}{T_1}-\frac{1}{T_2}\right) \quad (5)$$

where T_1 and T_2 are two generic absolute temperatures.

From eq. (5) it follows that a semilogarithmic plot of $t_{1/2}$ half life decomposition with respect to the reciprocal of absolute temperature $1/T$ is a straight line with angular coefficient equal to $-E_a/R_g$. Law (5) is commonly used by practitioners to have an idea of the peroxide to use in the manufacturing process. As a rule, engineers know approximately exposition time (which is a known parameter when cable velocity and vulcanization tube length are fixed) and nitrogen temperature T_s. From exposition time, peroxide to use is normally selected multiplying exposition time by 0.3, hence finding $t_{1/2}$ half life decomposition of the plant. In this way, a restricted number of commercial peroxides are selected. Considering also that the maximum value of the temperature profile for external rubber layers is usually not far from T_s, manufactures experience drives the final choice of the peroxide to use.

Cable tensile strength and tear resistance

Vulcanized rubber and thermoplastic elastomers (TPE) often fail in service because of the generation and propagation of special type of ruptures, called "tear", with elastoplastic and even fragile phenomena. Other usual failures that produce enormous economical losses and that manufactures aim to avoid is those due to the lack of tensile strength, which for

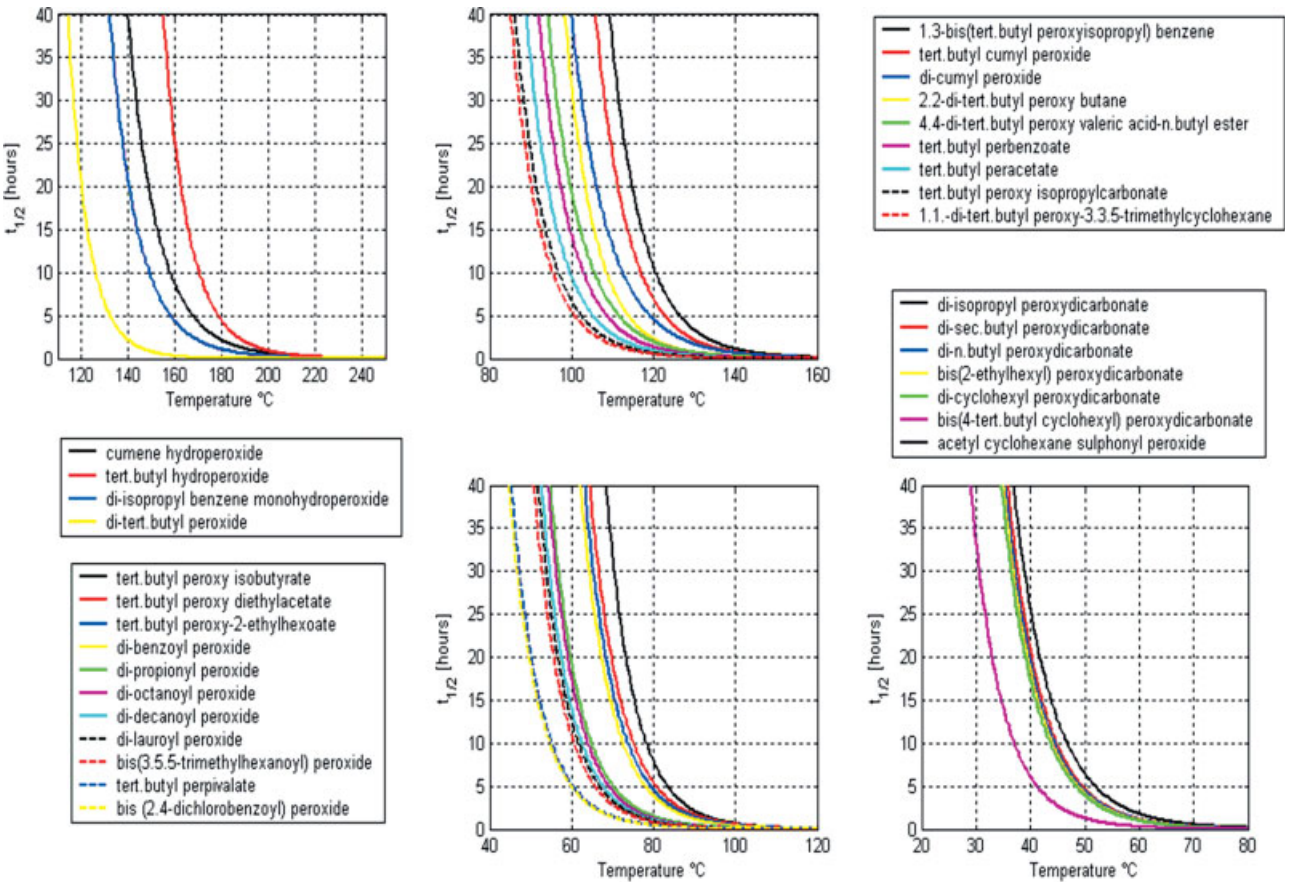

Figure 7 Commercial peroxides temperature $t_{1/2}$ curves. [Color figure can be viewed in the online issue, which is available at www.interscience.wiley.com.]

instance causes dangerous water infiltrations even in service conditions. Therefore, among the other mechanical properties, both tensile strength σ_t[29] and tear resistance F_t[30] are crucial output parameters for producers to check at the end of the production line.

On the other hand, it is well known that rubber output mechanical properties depend on a number of concurring factors, among the others the most important being the degree of vulcanization, which is itself a consequence of curing temperature, curing time and chemical reactions occurring between the number of compounds present in the rubber. As well known, such chemical reactions are variable from case to case and involve only a few atoms in each polymer molecule.

As stated theoretically[6] and experimentally,[8] the C_0 amount of peroxide added at the beginning of the vulcanization is always chosen with the aim of maximizing elastic properties of the items (rebound, tension set, heat built up in a compression flexion test, elongation, and hardness). All such parameters depend in a monotonic way with respect to the extent of vulcanization, thus depending monotonically on peroxide concentration C_0 (i.e., elastic properties reach asymptotically a maximum or a minimum increasing C_0). As a consequence, C_0 is always a fixed input parameter (typical values of C_0 used also in this article for the different peroxides inspected are reported in Ref. 6). On the other hand, inelastic properties, as for instance tensile and tear strength, do not increase monotonically with respect to curing time, thus requiring an optimization with respect to nitrogen temperature and exposition time.

Experimental tests conducted on EPM/EPDM rubber using a number of different peroxides (see Hofmann 8 and also Refs. 5, 7) showed that rubber macroscopic mechanical properties (tear resistance, elongation, tensile strength, Young modulus, etc.) can be regarded as dependent on C/C_0 ratio, where C denotes the concentration of unreacted peroxide C_0, see Figure 8. Since peroxide concentration depends on curing time via half life $t_{1/2}$ parameter [see eq. (3)] and $t_{1/2}$ is a function of absolute temperature T, it appears clear that rubber macroscopic mechanical properties are dependent on curing time (see Ref. 8) in a nontrivial way.

An excess in curing time usually results in a slight decrease of final strength, as shown in Figure 9(a) and in.[8] Tear resistance[30] has a similar behavior,[8,5,7] except for a more marked nonlinear branch at low

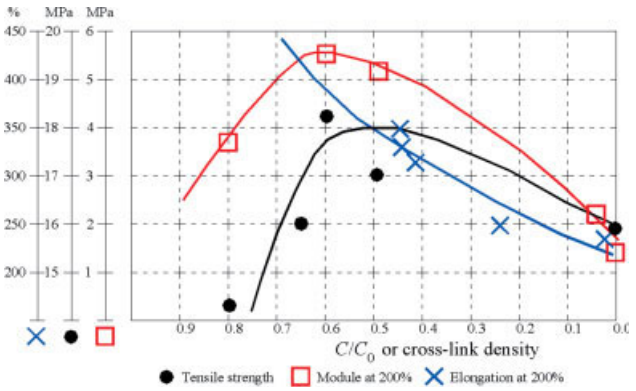

Figure 8 Nonlinear behavior of output rubber mechanical properties with respect to peroxide unreacted concentration (data processed from Hofmann experimentation 8). [Color figure can be viewed in the online issue, which is available at www.interscience.wiley.com.]

levels of unreacted peroxide, Figure 9(b). The different values of concentration at which functions reach their maximum is worth noting, see Figure 9. In an equivalent way, tensile and tear strength are also function of cross-link density, being C/C_0 a measure of cross-linking, Figure 9.

In Figure 10, rubber behavior vulcanized with dicumyl peroxide is shown as a function of temperature and exposition time. In particular, in Figure 10(a) tensile strength function is reported, whereas in Figure 10(b) unreacted peroxide concentration is plotted as a function of T and t. As it is possible to notice, Figure 10(a), optimal tensile strength is reached only at particular values of T and t. Obviously, such a representation is able to give correct information on output parameters only at constant temperatures (note that $T \neq T_s$, T being rubber temperature), i.e., assuming that each layer of the insulator in the cable withstands the same temperature at different time steps, which obviously is quite unrealistic for the case considered here. As well known, in fact, real nonconstant temperature profiles $T = T(t)$ for each layer has to be determined solving a suitable differential system, as it will be shown in what follows.

BASIC SCHEMES OF THE MATHEMATICAL MODEL ADOPTED

As a matter of fact, experimental evidences show that nitrogen temperature to adopt depends on the peroxide used for the reticulation of EPDM. Velocity of the cable is another key aspect which determines (once that a production line length is a priori assumed) the exposition time.

Optimal EPDM mechanical properties in terms of tear strength and tensile ultimate stress lead to a nontrivial optimization problem that, if suitably solved, is able to give essential information on the performance maximization of the production line.

The pseudo-code of the algorithm used for the optimization of the production line is summarized in Figure 11. Code was entirely developed in Matlab[31] language. The following steps are repeated in the code at different nitrogen temperatures and exposition time:

1. Determination of temperature profiles along cable thickness. At this aim, heat transmission Fourier law in cylindrical coordinates[28] is used in the conductor layer j and in the insulator layer p. As it will be shown in what follows, a nontrivial partial differential equation system is obtained. An efficient numerical strategy based on a finite differences approach is used to numerically tackle the problem.
2. Determination of insulator mechanical properties at different temperatures and different exposition times. As experimental evidences

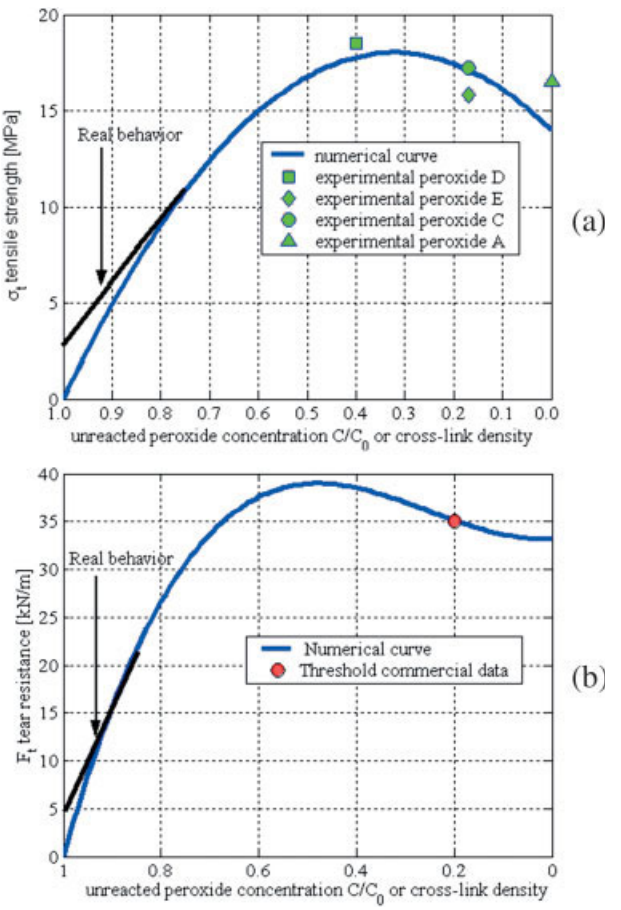

Figure 9 (a) quadratic interpolation of experimental data, tensile strength-unreacted peroxide concentration data. (b) cubic function for rubber tear resistance-unreacted peroxide concentration. [Color figure can be viewed in the online issue, which is available at www.interscience.wiley.com.]

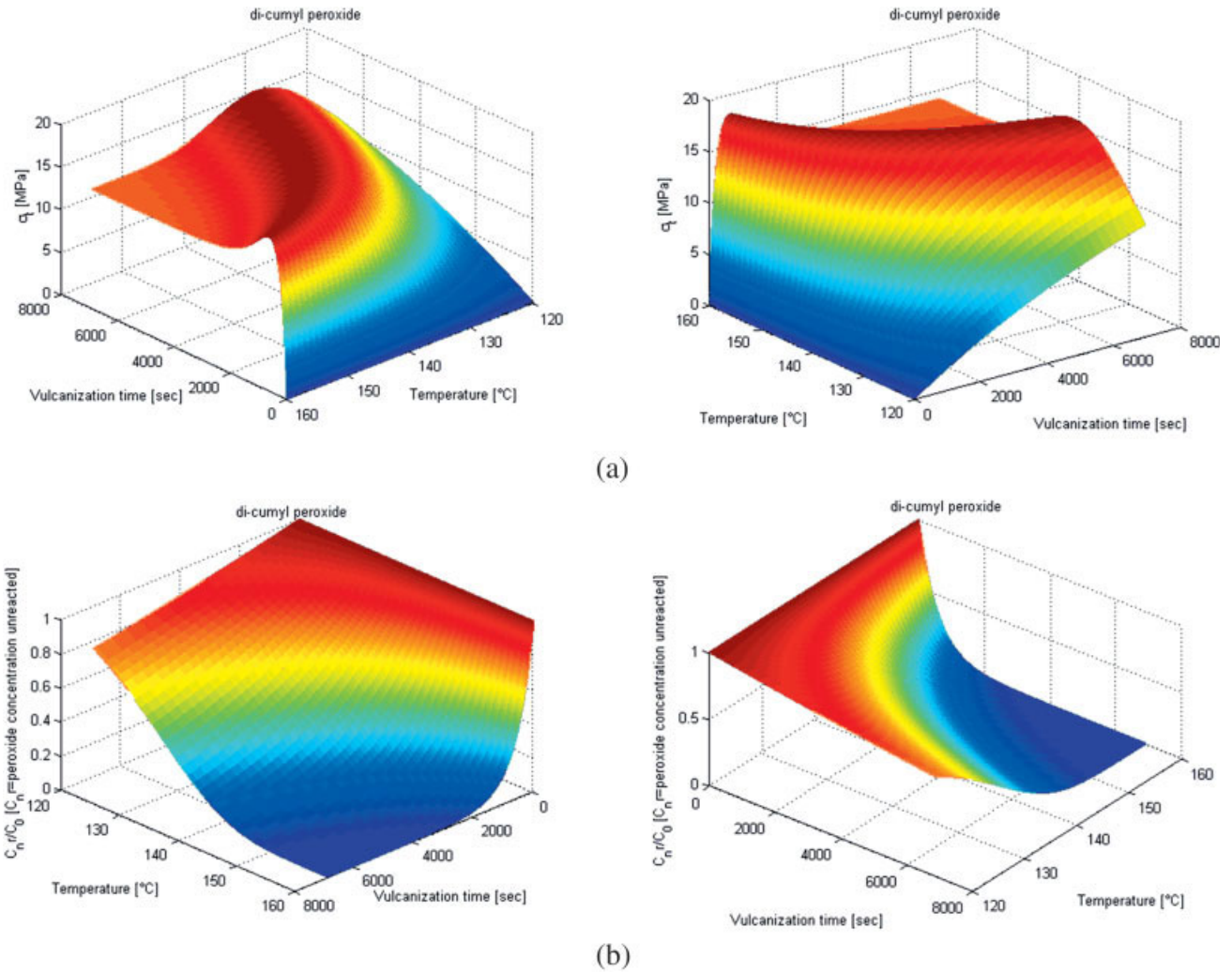

Figure 10 Di-cumyl peroxide. (a) tensile strength at different rubber temperatures and exposition times. (b) unreacted peroxide concentration at different temperature and exposition times. [Color figure can be viewed in the online issue, which is available at www.interscience.wiley.com.]

show, there is an optimal vulcanization time at different insulator fixed temperatures for which objective function (tensile stress, elongation, tear strength, etc.) is maximized. Depending on the radial position of the insulator layer considered, different temperature profiles are obtained from point (1), thus leading to slightly different mechanical properties along the cable thickness. In the article, an averaged objective function is adopted (i.e., the mean tensile stress/tear resistance is maximized). Nevertheless, it is worth noting that no conceptual difficulties arise if the internal or external layer tensile stress/tear resistance has to be maximized.

3. Determination by means of nonstandard GA procedures of an optimal (T_i t_i) input individual (i.e., nitrogen temperature-exposition time pair) which maximizes output insulator mechanical properties.

Governing partial differential equations

The vulcanization process can be schematically subdivided into three separate phases: in the first phase, the cable is exposed to high temperatures by means of nitrogen flow, in the second step a cooling phase with water is applied and finally air is used for a further cooling. In some cases, only water or air is used in the cooling phase.

Let us consider a cable composed with a conductor j of ray R_j and an insulator p with ray R_p, Figure 2. Since the ratio between cable length and diameter is around 2000–8000 and due to the axial symmetry of the problem, it is possible to model the process by means of only two independent variables, i.e., the distance r of a layer in the insulator with respect to cable axis and exposition time t. It is interesting to note that, being cable velocity u_c constant, a cable section at a distance z with respect to the starting point of the production line, is characterized by an exposition

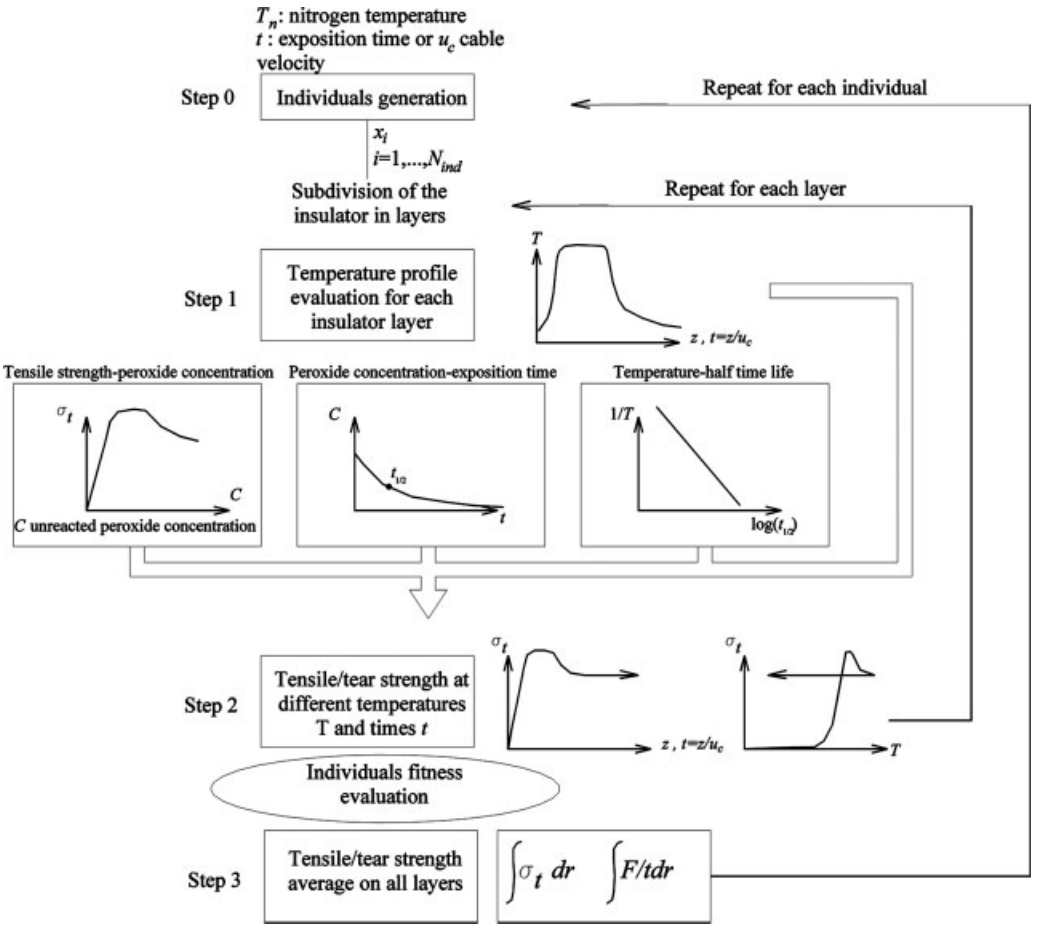

Figure 11 Schematic representation of the optimization process phases.

time equal to $t = \frac{z}{u_c}$, meaning that z is a dependent variable. Thus, for each layer of the cable at a distance r to the centre, it is possible to rebuild its temperature profile with respect to exposition time, i.e., at different positions z in the production line.

During the heating phase, nitrogen at constant temperature T_s is used, exchanging heat with EPDM external surface by radiation and convection. Temperature profiles along cable thickness are obtained solving numerically a partial differential equations system problem. At this aim, Fourier's heat equation law in cylindrical coordinates is used.[28] In particular, for the insulator, the heat balance field equation is the following:

$$\rho_p c_p^p \left(\frac{\partial T}{\partial t}\right) - \lambda_p \left(\frac{\partial^2 T}{\partial r^2} + \frac{1}{r}\frac{\partial T}{\partial r}\right) - r_p \Delta H_r = 0 \qquad (6)$$

where ρ_p, c_p^p, and λ_p are EPDM density, specific heat capacity and heat conductivity, respectively; ΔH_r is the insulator specific heat (enthalpy[32]) of reaction and is expressed in kJ/mol; r_p is the rate of cross-linking and is expressed in mol/(m^3 sec).

It is worth noting that the term $r_p \Delta H_r$ in eq. (6) is the heat required by the decomposition of the peroxide. ΔH_r, usually ranging from 120 to 180 kJ/mol, represents the bone breaking between oxygen-oxygen in the peroxide. As a rule, $r_p \Delta H_r$ depends both on T and t and several models can be used for an analytical definition of r_p function. Nonetheless, for the sake of simplicity we assume here a linear behavior for r_p with respect to concentration t derivative. More complex relations can be adopted[28] in the model proposed without any numerical difficulty. In any case, the contribution of such a term in the heat exchange eq. (6) is small and depends on peroxide concentration in the mixture, which usually is around 1–2% with respect to the blend used.

Analogous considerations can be done for the conductor, except that in this case there is no heat produced from chemical reactions (i.e., $\Delta H_r = 0$):

$$\rho_j c_j^p \left(\frac{\partial T}{\partial t}\right) - \lambda_j \left(\frac{\partial^2 T}{\partial r^2} + \frac{1}{r}\frac{\partial T}{\partial r}\right) = 0 \qquad (7)$$

where all the symbols have been already introduced and the index j refers to the conductor layer.

Initial and boundary conditions

Heat equation is of second order in space; hence, two boundary conditions must be specified. For the problem at hand, at $r = 0$:

$$\frac{\partial T}{\partial r} = 0 \tag{8}$$

which is a symmetry condition on the temperature field, whereas at $r = R_p$

$$\lambda_p \frac{\partial T}{\partial t} + h\left(T\left(R_p, t\right) - T_s\right) + q_{rad} = 0 \tag{9}$$

where h denotes the heat transfer coefficient between EPDM and nitrogen, T_s is the nitrogen temperature, and q_{rad} is the heat flux transferred by radiation, which can be evaluated applying the well known following formula:

$$q_{rad} = \sigma\left(T_s^4 - T\left(R_p, t\right)^4\right) \Big/ \left[1/\varepsilon_p + \frac{A_p}{A_n}(1/\varepsilon_n - 1)\right] \tag{10}$$

assuming $\sigma = 5.67 \times 10^{-8} \frac{W}{m^2 K^4}$ (Stefan-Boltzmann constant). $\varepsilon_{p,n}$ in (10) are emissivity coefficients and $A_{p,n}$ is the areas of heat exchange (p: insulator, n: nitrogen).

Finally, at the interface between conductor and insulator, heat flux exchanged is in equilibrium, meaning that

$$\lambda_j \frac{\partial T\left(R_j - \varepsilon, t\right)}{\partial r} = \lambda_p \frac{\partial T\left(R_j + \varepsilon, t\right)}{\partial r} \quad \varepsilon \to 0 \tag{11}$$

For transient conduction, heat equation is of first order in time, requiring the assumption of an initial temperature distribution:

$$\begin{aligned} T(r,0) &= T_j^0 \quad 0 \le r < R_j \\ T(r,0) &= T_p^0 \quad R_j \le r \le R_p \end{aligned} \tag{12}$$

No differences occur in the cooling zone, except that boundary eq. (9) is replaced by the following expression:

$$\lambda_p \frac{\partial T}{\partial r} + h_w\left(T\left(R_p, t\right) - T_w\right) = 0 \tag{13}$$

where h_w is the water heat transfer coefficient and T_w is the water cooling temperature.

Initial conditions on temperature are obtained from the profile evaluated at the last step of the cooling zone, i.e., at $T(r,t_c)$, where $t_c = L_h/u_c$ with L_h curing zone length. Obviously, if a cooling phase with air is added, similar consideration can be repeated without particular conceptual difficulties.

The resulting partial differential equations system is solved by means of a finite differences scheme (namely the method of lines, see Refs. 33–35 for details). In all the numerical simulations proposed, the following general parameters have been used, see Seymour and Krick[17]: EPM/EPDM density ρ_p = 1180 Kg/m^3, insulator specific heat capacity c_p^p = 1700 J/(Kg °C), λ_p = 0.26 W/(m °C), conductor density ρ_j = 2707 Kg/m^2, conductor specific heat capacity c_j^p = 896 J/(kg °C), λ_j = 206 W/(m °C), ΔH_r = 180 kJ/mol, water heat transfer coefficient h_w = 1490.70 W/(m^2 °C), nitrogen heat transfer coefficient h = 900 W/(m^2 °C), $\varepsilon_p = 0.60$, $\varepsilon_n = 0.70$, water cooling temperature $T_w = 25$°C.

Activation energy E_a and $k_{\max}$ depend on the peroxide used, eq. (4). h_w and h should be derived from well known empirical formulas related to laminar/turbulent flow of fluids, see Ref. 28 for details, nevertheless here characteristic values are used for the sake of simplicity. In Figure 12(a), a typical temperature profile for the insulator with di-cumyl peroxide at different exposition times and radial distances is shown. The following parameters have been used: R_p = 18.8 mm, R_j = 8 mm, T_s = 200°C, T_w = 25°C, L_h = 1/2 L_w = 40 m. In all the simulations which follow, we define as "exposition time" the time needed for each section of the cable to pass through $L_h + L_w$ length. Therefore, curing time can be obtained multiplying exposition time by 1/3.

A section at $r = \tilde{r}$ = constant of Figure 12(a) allows to know temperatures of layer $\tilde{r}$ at increasing times, i.e., $T = T_{\tilde{r}}(t)$. By means of the relation $T = T_{\tilde{r}}(t)$, $t_{1/2}(T)$ and $C(t)$ can be determined, respectively from eqs. (5) and (3). Once that $C(t)$ is known, Figure 9, both σ_t and F_t can be plotted for layer $\tilde{r}$ as a function of temperature profile and exposition time. For example, in Figure 12(b), $\sigma_t - t$ curve is shown assuming $\tilde{r} = R_j$, whereas in Figure 12(c) the corresponding $\sigma_t - T$ function is depicted. As one can note, it is particularly evident the presence of an optimal $t - T$ point at which σ_t reaches its maximum for the layer considered, which corresponds to a specific value of unreacted peroxide concentration in the mixture [Fig. 12(d)].

THE GENETIC ALGORITHM PROPOSED

In this section, a genetic algorithm with zooming tool, specifically developed for the optimization of power cables production lines, is presented.

The advantage related to the utilization of a GA is represented by (a) the theoretical simplicity of the procedure itself, (b) the robustness and efficiency in terms of time required for the optimization, and (c) its application to the case in which objective function is not known analytically. For the problem at hand, point (c) is crucial, leading to prefer stochastic and/or metaheuristic approaches instead of classic methods. In fact, in this case, temperature profiles (which give by integration the objective function) are derived from a finite differences numerical solution of a PDEs system,

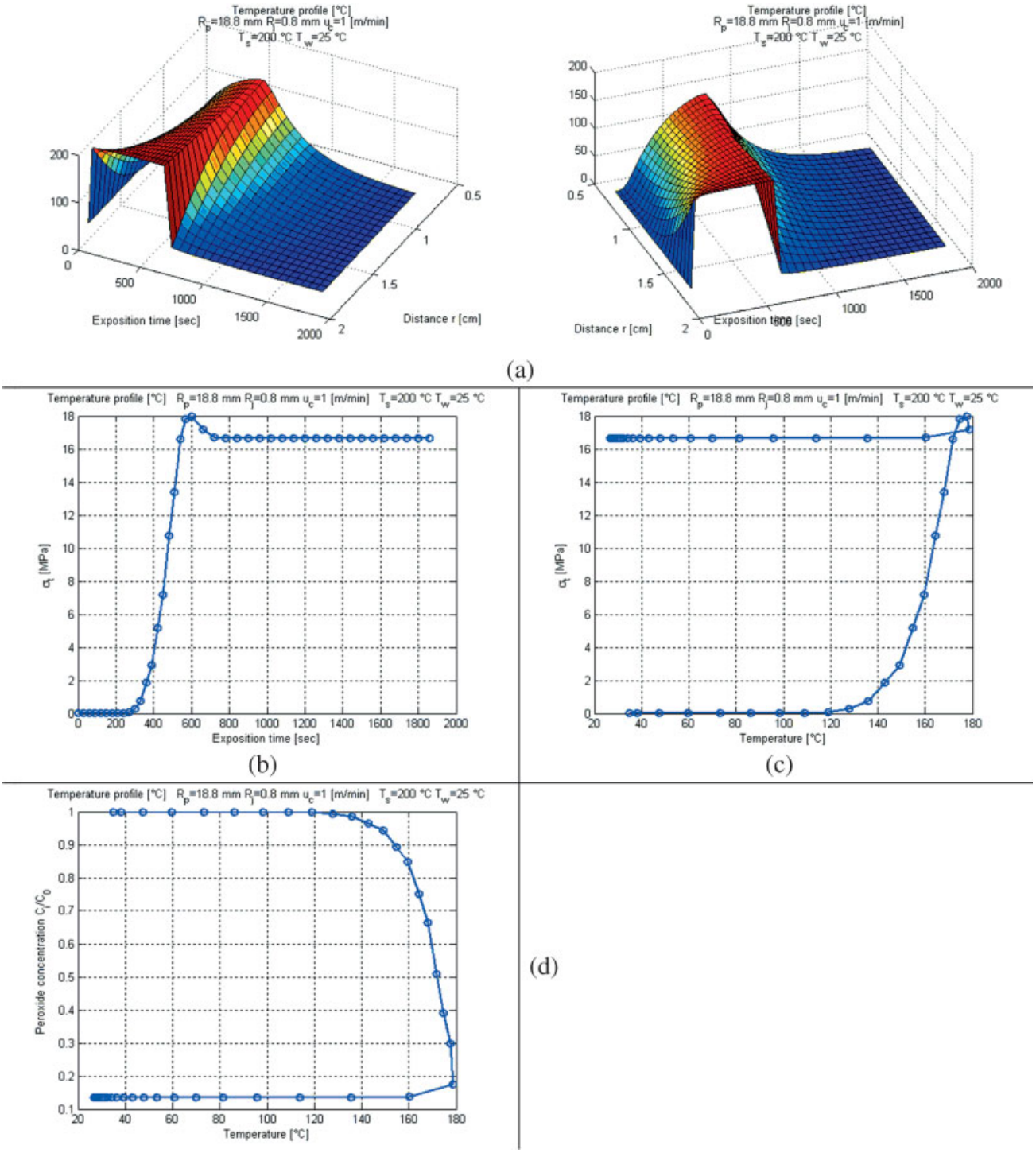

Figure 12 (a) Typical temperature profile along insulator thickness. (b) Typical $\sigma_t - t$ curve ($\tilde{r} = R_p$). (c) Typical $\sigma_t - T$ curve ($\tilde{r} = R_p$). (d) peroxide concentration C- temperature T curve. [Color figure can be viewed in the online issue, which is available at www.interscience.wiley.com.]

thus leading to a nonlinear optimization problem in which objective function is not analytically known.

The GA algorithm here proposed, see Goldberg,[36] classically operates on a population of potential solutions applying the principle of survival of the fittest to produce better and better approximations to a solution. At each generation, a new set of approximations is created by the process of selecting individuals according to their level of fitness in the problem domain and breeding them together using operators borrowed from natural genetics. This process leads to the evolution of populations of individuals that are better suited to their environment than the individuals that they were created from.

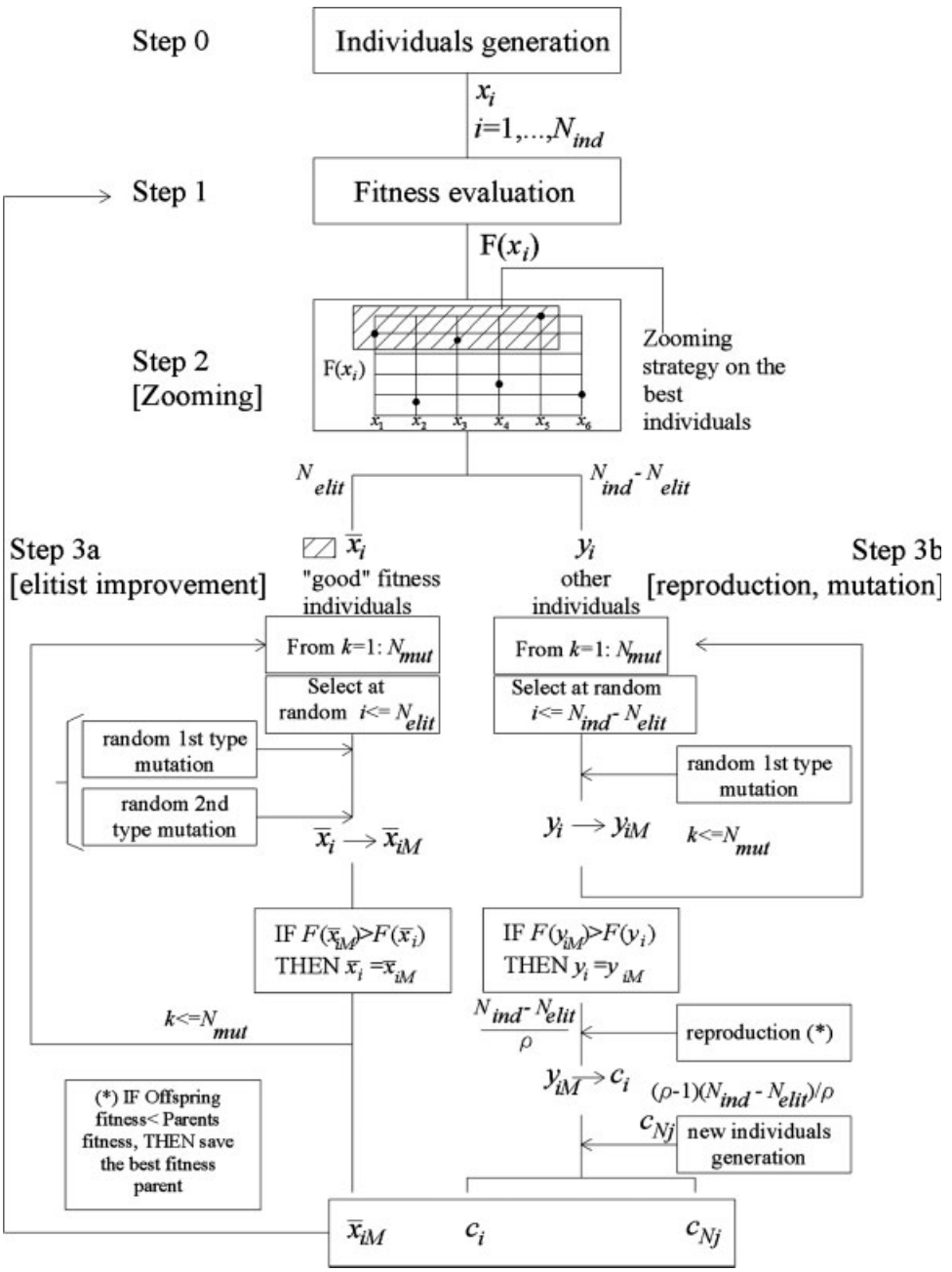

Figure 13 Pseudo-code of the GA proposed.

The kernel of the GA proposed is a set of standard genetic operations consisting of reproduction, crossover, and mutation and nonstandard procedures, such as zooming and elitist strategy. Each individual is represented by an admissible temperature and exposition time, i.e., a sequence of individuals i in the form (T_s^i t^i). Since individuals are stored as a sequence of two real positive numbers, their encoding by means of binary strings results particularly simple. In this way, the genotypes (chromosome values) can be uniquely mapped onto the decision variable (phenotypic) domain. In a standard GA, the use of Gray coding is necessary to avoid a hidden representational bias in conventional binary representation as the Hamming distance between adjacent values is constant (see Holstien[37] and Haupt and Haupt[38]):

The kernel of the GA proposed consists of an assemblage of both standard operators (reproduction, crossing-over, and mutation) and nonstandard strategies (subdivision of the population into two subgroups with improvement of the best fitness individuals with zooming[39–41]), summarized in the following steps (Fig. 13):

Step 0: an admissible initial population $\mathbf{x} = \{x_i : i = 1,\ldots, N_{ind} \mid x_i \text{ admissible}\}$ is randomly generated at the first iteration.

Step 1: x_i fitness $F(x_i)$ is evaluated solving for each layer a PDEs system with fixed x_i;

Step 2: two sub groups are created denoted as $\overline{\mathbf{x}} = \{\overline{x}_i : i = 1,\ldots, N_{elit} \mid x_i \text{ admissible}\}$ and $\mathbf{y} = \mathbf{x} - \overline{\mathbf{x}} = \{y_i : i = 1,\ldots, N_{ind} - N_{elit}\}$, such that $\overline{\mathbf{x}}$ is the group of all the individuals with the N_{elit} (user defined) higher fitness values (zooming strategy).

Step 3a: for each $\overline{x}_i$, a random improvement of the individual (in terms of fitness) is tried, by means of two different mutation operators (first and second type, as described in what follows and as illustrated in Fig. 13). The recursive double operation (applied randomly N_{mut} times) leads to new individuals generation ($\overline{x}_{iM}$), which overwrite the original $\overline{x}_i$ only if their fitness $F(\overline{x}_{iM})$ is greater than $F(\overline{x}_i)$. At the end of the double loop, a new subgroup $\overline{\mathbf{x}}_M = \{\overline{x}_{iM} : i = 1,\ldots, N_{elit} \mid \overline{x}_{iM} \text{ admissible}\}$ is obtained.

Step 3b: for each y_i, a mutation loop (only first type mutation) is applied randomly N_{mut} times, leading to an improvement of y_i fitness. The new individuals y_{iM} overwrite the original y_i only if their fitness is greater than y_i one (elitist approach). At the end of the double loop, a new subgroup $\mathbf{y}_M = \{y_{iM} : i = 1,\ldots, N_{\text{ind}} - N_{\text{elit}} \mid y_{iM} \text{ admissible}\}$ is obtained. A classic reproduction operator is applied only for individuals of $\mathbf{y}_M$ with high fitness (i.e., on $(N_{\text{ind}} - N_{\text{elit}})/\rho$ parents with user defined parameter $\rho > 1$) to create a new offspring group $\mathbf{c}$. The remaining $(1 - \rho)\ (N_{\text{ind}} - N_{\text{elit}})/\rho$ individuals are generated *ex-novo* using Step 0 procedure and are catalogued into $\mathbf{c}_N = \{c_{Nj} : j : 1,\ldots, (N_{\text{ind}} - N_{\text{elit}})\ /\ \rho \mid c_{Nj} \text{ admissible}\}$.

Step 4: the final population at the ith iteration is collected into $\mathbf{x} = [\overline{\mathbf{x}}_M\ \mathbf{c}\ \mathbf{c}_N]$ and the procedure is repeated from Step 1 with a fixed number of iterations. As a rule, maximum number of iterations does not exceed 40, thus demonstrating that the procedure is not time consuming.

It is worth noting that the implementation in the code of *ad hoc* nonstandard strategies (zooming with elitist strategy) is necessary to obtain a considerable enhancement of both robustness and efficiency of the algorithm.

Generation of admissible individuals

The generation of admissible individuals occurs by means of random processes respecting all admissibility conditions ($T_s > 0$ and $t > 0$). Such a procedure is followed at the first iteration (for all the N_{ind} individuals) and at each iteration $i > 1$, see Figure 13, for $(\rho - 1)\ (N_{\text{ind}} - N_{\text{elit}})/\rho$ individuals. A binary representation with chromosomes is used for each individual in the population. If, as is the case here treated, the number of optimization variables (here denoted as N_{var}) is 2 (i.e., a 2D optimization problem in T_s and t has to be solved) each individual is represented by $N_{\text{bit}} = N_{\text{bit}}^1 + N_{\text{bit}}^2$ chromosomes.

Thus, the population has N_{bit} chromosomes and is an $N_{\text{ind}}xN_{\text{bit}}$ matrix filled with random ones and zeros generated using (see Ref. 38) the following syntax:

$$\text{pop} = \text{round}(\text{rand}(N_{\text{ind}}, N_{\text{bit}})) \tag{14}$$

where the function rand(N_{ind},N_{bit}) generates a $N_{\text{ind}}xN_{\text{bit}}$ matrix of uniform random numbers between zero and one. The function round rounds the numbers to the closest integer which in this case is either 0 or 1. Each row in the pop matrix is obviously an individual encoded with chromosomes. The chromosomes correspond to discrete values of nitrogen temperature and exposition time. To pass from a binary representation to a continuous representation, a so called quantization error is introduced. Obviously, increasing the number of bits reduces the quantization error. Furthermore, an upper bound limitation is introduced for T_s and t variables, assuming for all the examples treated that $T_s < T_s^{\max} = 400^\circ\text{C}$ and $t < t^{\max} = 25{,}200$ s $= 7$ h. In fact, unbounded variables should require, at least from a theoretical point of view, an infinite number of bits for their encoded representation. In what follows, to introduce a negligible quantization error, a $N_{\text{bit}} = 64$ bits representation is used for individuals (only 16 bits are utilized for temperature whereas the remaining are allocated for time, being temperature range smaller with respect to exposition time range). Next, the variables are passed to the cost function for evaluation. As a rule, small populations are utilized in the optimization process, constituted by around $N_{\text{ind}} = 30 - 40$ individuals.

Reproduction

The reproduction phase is applied to $y = \{y_i : i = 1,\ldots,N_{\text{ind}} - N_{\text{elit}}\}$ group. As usual, for each individual, a fitness value derived from its raw performance measure given by the objective function is assigned. This value is used in the selection to bias towards more fit individuals. Highly fit individuals, relatively to the whole population, have a high probability of being selected for mating whereas less fit individuals have a correspondingly low probability of being selected.

Once the individuals have been assigned a fitness value, they can be chosen from the population, with a probability according to their relative fitness, and recombined to produce the next generation.

For the selection operator, a stochastic sampling with replacement (roulette wheel, see Ref. 36, 39) is utilized. An interval I is determined as the sum of the fitness values F_i of all the individuals in the current population, i.e., $I = \sum F_i$. For each individual i, a subinterval S_i corresponding to its fitness value in the interval [0, I] is determined, i.e., $S_i = F_i$, so that $I = \sum S_i$ and the size of the interval associated to each individual is proportional to its fitness, i.e., so that a big subinterval corresponds to a highly fit individual. To select an individual, a random number is generated in the interval [0, I] and the individual whose segment subinterval spans the random number is selected. This process is repeated until the desired number of individuals have been selected.

Reproduction is active only on $\mathbf{y}$ subpopulation. Only an offspring per pair is generated and a total number of $(N_{\text{ind}} - N_{\text{elit}})/\rho$ of reproductions is allowed. The remaining $(\rho - 1)$ $(N_{\text{ind}} - N_{\text{elit}})/\rho$ individuals are generated *ex-novo*.

Zooming and elitist strategy

The application of an *ad hoc* technique for the problem at hand is required to obtain improved and reliable results in terms of best fitness at each iteration. As already pointed out, the kernel of the algorithm relies in subdividing the initial population into two groups:

$$\begin{aligned} \bar{\mathbf{x}} &= \{\bar{x}_i : i = 1, \ldots, N_{\text{elit}} | x_i \text{ admissible}\} \\ \bar{\mathbf{y}} &= \mathbf{x} - \bar{\mathbf{x}} = \{y_i : i = 1, \ldots, N_{\text{ind}} - N_{\text{elit}}\} \end{aligned} \tag{15}$$

The so called zooming strategy consists in collecting at each iteration the individuals with higher fitness into an "elite" subpopulation $\bar{\mathbf{x}}$ (with user defined dimension N_{elit}). Then, for each individual belonging to group $\bar{\mathbf{x}}$, only mutation (with high probability) is applied to improve individuals fitness. Two different mutation algorithms are utilized, differing only on the number of cells of each individual involved by the mutation process.

Subsequently, an elitist strategy preserves the original individual if mutation results in a reduction of individual fitness, whereas zooming technique restricts search domain, so improving in any case convergence rate. Unfortunately, no theorems are available for assuring an unconditioned convergence of the method in any case, as well as no theoretical rules can be given in the choice of both reproduction and mutation schemes. As a consequence, only experience in the numerical simulations of specific problems can help in the correct choice of input parameters (see Ref. 39–41).

Zooming has to be a priori set by the user by means of the so called zooming percentage $z_{\%}$ defined as the percentage ratio between $\mathbf{x}$ initial population and $\bar{\mathbf{x}}$ subpopulation dimension, i.e., $z_{\%} = \frac{N_{\text{elit}}}{N_{\text{ind}}} 100$.

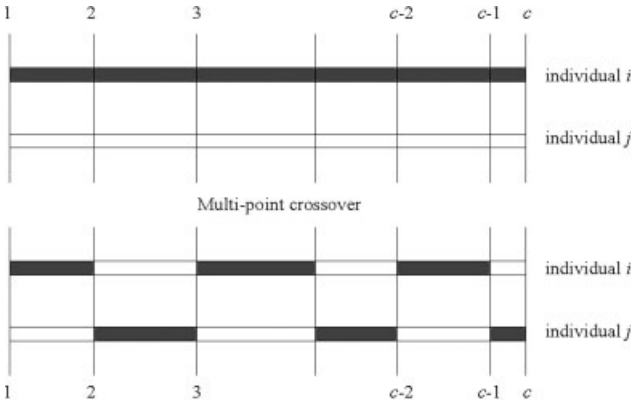

Figure 14 Multi point crossover.

Crossover

During a generation of a new individual from two parents, a crossover operator is used to exchange genetic information between pairs. In the present study, we use a multipoint crossover operator, which works as follows: $k_i = [1, 2, \ldots, c - 1]$ crossover points are randomly selected on two individuals (parents) represented by c chromosomes (bits), as shown in Figure 14. Bits between the crossover points are then exchanged between the parents to produce a new offspring.

Mutation

Mutation is generally considered to be a background operator that ensures that the probability of searching a particular subspace of the problem space is never zero. In the present algorithm, mutation is applied with high probability directly on existing individuals and two different algorithms (here denoted as first and second type) are applied. Mutation is a fundamental task that permits a strong fitness improvement at each iteration.

First type mutation

Such operator is the classic mutation and is applied both on $\bar{\mathbf{x}}$ and $\mathbf{y}$ individuals. For each individual $\bar{\mathbf{x}}_i$ (or $\mathbf{y}_i$) it works stochastically on all the chromosomes (i.e., changing at random one of the individual columns from 1 to N_{bit}). The procedure is repeated 1 time on N_{mut} different individuals. Obviously, first type mutation results in a new individual in which only one of the optimization variables T_s and t, after chromosomes decoding, results changed with respect to the original individual.

Second type mutation

The second type mutation is applied only to $\bar{\mathbf{x}}$ individuals, to obtain a further improvement of their fitness. It works analogously to the first type algorithm, with the only difference that it changes, for the individual subjected to mutation, a chromosome belonging to T_s and one belonging to t. Thus, the resulting individual after chromosomes decoding is different from the original both in T_s and t. From a practical point of view, the GA proposed allows the user to perform both N_{mut} second type mutations or user defined N_{mut2} second type mutations. The final result of the application of both first and second type mutations is a new admissible individual (Fig. 13) $\bar{x}_{iM}$, with different fitness with respect to $\bar{x}_i$. As already pointed out, if $\bar{x}_{iM}$ fitness is higher than that of the original individual (note that the check is executed at each N_{mut} iteration), $\bar{x}_i$ is overwritten with $\bar{x}_{iM}$.

NUMERICAL SIMULATIONS

In this section, optimal input parameters functions $\hat{T} = \hat{T}(T_s, t) = 0 \,|\, \hat{T} \equiv \{P^i = (T_s^i, t^i)\text{optimal}\}$ are obtained by means of the GA approach proposed, for both medium and high voltage cables. Optimal $\hat{T}$ curves (expressed as implicit functions in T_s and t) are numerically evaluated solving point by point the following optimization problem:

$$\max \frac{1}{N_L}\sum_{k=1}^{N_L}\sigma_t^k(T_s^i,t^i) \text{ or } \max \frac{1}{N_L}\sum_{k=1}^{N_L}F_t^k(T_s^i,t^i)$$

$$\text{subject to} \begin{cases} 0 < T_s^i < T_s^{\max} \\ 0 < t^i < t^{\max} \end{cases} \text{PDEs system}$$

$$\times \begin{cases} \rho_j c_j^p\left(\dfrac{\partial T}{\partial t}\right) - \lambda_j\left(\dfrac{\partial^2 T}{\partial r^2} + \dfrac{1}{r}\dfrac{\partial T}{\partial r}\right) = 0 \\ \rho_p c_p^p\left(\dfrac{\partial T}{\partial t}\right) - \lambda_p\left(\dfrac{\partial^2 T}{\partial r^2} + \dfrac{1}{r}\dfrac{\partial T}{\partial r}\right) - r_p\Delta H_r = 0 \\ \text{boundary and initial conditions} \end{cases} \tag{16}$$

where N_L is the number of layers in which the insulator thickness is subdivided, k is the kth layer, and $T_s^{\max}(t^{\max})$ is an upper bound limitation for nitrogen temperature (exposition time).

Four peroxides are tested, to show the differences (in terms of output parameters) occurring using different $t_{1/2} - T$ relations: dicumyl peroxide, 1.1 bis(t.butyl-peroxy)-3.3.5 trimetylcyclohexane (here denoted for brevity peroxide A), $\alpha - \alpha'$-bis-(t-butylperoxy)-diisopropylbenzene (peroxide D) and 2.5-dimethyl-2.5-bis-(t-butylperoxy)-hexan (peroxide E) are critically analyzed. Furthermore, the results provided by the GA approach proposed are compared with those obtained subdividing $T_s - t$ plane with a regular grid. For each point $P^{i,j} \equiv (T_s^i, t^j)$ of the grid a mixed algebraic-PDEs system has to be solved:

$$\sigma_t = \frac{1}{N_L}\sum_{k=1}^{N_L}\sigma_t^k(T_s^i,t^i)$$

$$F_t = \frac{1}{N_L}\sum_{k=1}^{N_L}F_t^k(T_s^i,t^i)$$

$$\text{PDEssystem} \begin{cases} \rho_j c_j^p\left(\dfrac{\partial T}{\partial t}\right) - \lambda_j\left(\dfrac{\partial^2 T}{\partial r^2} + \dfrac{1}{r}\dfrac{\partial T}{\partial r}\right) = 0 \\ \rho_p c_p^p\left(\dfrac{\partial T}{\partial t}\right) - \lambda_p\left(\dfrac{\partial^2 T}{\partial r^2} + \dfrac{1}{r}\dfrac{\partial T}{\partial r}\right) - r_p\Delta H_r = 0 \\ \text{boundary and initial conditions} \end{cases} \tag{17}$$

A relatively large computational effort is required in solving problem (17). For instance, when a 30×30 coarse mesh is used (as is the case of the simulations reported in what follows), a processing time of almost 4 h is required for each simulation on an Intel Celeron 1.4 GHz equipped with 512 MB ram. On the contrary, the GA approach presented required only 3–6 min to process optimal curves for all the cases analyzed (depending on the number of points desired on the curve, fixed from 10 to 30 by the authors and the number of generations required for the optimization, which typically, being based on stochastic processes, varies from 10 to 50). The evident advantage in terms of processing time obtained using the GA proposed is worth noting.

From the results of the numerical simulations, the following aspects have to be underlined: The utilization of different peroxides influences optimal $\hat{T}$ extensively. Therefore, it appears particularly useful the numerical determination of $\hat{T}$ functions for each peroxide. At this aim, $\hat{T}$ curves obtained numerically are reported in 2D figures for all the peroxides analyzed, which can be directly utilized for practical purposes, allowing the almost immediate determination of the most suitable (T_s^i, t^i) parameters for each peroxide analyzed.

Optimal curves obtained assuming as objective function tensile strength differ visibly from those obtained assuming as objective tear resistance, depending on the peroxide used but especially for nitrogen temperatures $< 180°C$. This is an obvious consequence of the fact that tear and tensile strength reach a maximum at different values of unreacted peroxide. Such a behavior demonstrates that the objective function choice is the crucial criterion for the optimization of the production line process.

Tensile and tear strength optimization with respect to nitrogen temperature and exposition time for different peroxides used

For all the numerical simulations reported in this section, the following GA parameters have been used: number of individuals $N_{\text{ind}} = 30$, zooming $z_{\%}$ 30%, total number of first and second type mutations $N_{\text{mut}} = 8$, parameter ρ equal to 0.5, maximum number of generations $N_{\text{gen}} = 40$–60.

From the above mentioned parameters and from a comparison between GA approach and classic expensive analysis with regular grids (see for instance Fig. 15), it is particularly evident the reliability of the procedure proposed. From a practical point of view, a micro-GA approach is adopted, meaning that the nonstandard procedure presented is reliable even with a very limited number of individuals in the population (the efficiency is improved for the introduction of the ad hoc zooming/elitist strategy).

In Figure 15, rubber output mechanical properties at different temperatures and exposition times are reported for medium voltage cables, assuming as reticulation inducer di-cumyl-peroxide. In particular, in Figure 15(a) rubber mean tensile strength is represented. The 3D surface is obtained with an expensive regular grid of points obtained solving (17), whereas green squares are the inexpensive GA optimization points. As it is possible to notice, the algorithm proposed is able to reach tensile maximum strength with sufficient accuracy for all the simulations performed.

In Figure 15(b) the same simulations are reported for tear resistance. In this case, GA optimization points are represented by red circles. Finally, in Figure 15(c) optimal tear resistance/tensile strength exposition time-temperature curves (i.e., $\hat{T}$ functions) are represented. As it is possible to argue from Figure 15(c), optimal curves of tensile and tear strength do not coincide. Especially for low values of nitrogen temperature, optimal exposition times are quite different, meaning that Pareto frontiers[11] should be recovered case by case.

The same simulations reported in Figure 15 for medium voltage cables are repeated in Figure 16 for high voltage wires. A comparison between Figures 15 and 16 clearly demonstrates that optimized curves are quite different, meaning that insulator thickness plays a crucial role. As experimental evidences show, in fact, insulator thickness changes temperature profiles, therefore changing both optimal nitrogen temperature and optimal exposition time.

The same simulations reported in Figures 15 and 16 are reported from Figures 17 to 22 for peroxide A (Figs. 17 and 18), peroxide D (Figs. 19 and 20) and peroxide E (Figs. 21 and 22) respectively in presence of both medium and high voltage cables.

A detailed comparison among all the aforementioned results shows that peroxide choice is crucial. Each peroxide, in fact, has a different $t_{1/2}(T)-t$ behavior and, in some cases, such characteristic curves are sensibly different. Obviously, this results in completely different optimal curves for the production line [compare, for instance, Figs. 19(c) and 17(c)].

Combined optimal tear and-tensile strength: Pareto frontiers

In this section, a multi objective optimization problem in which both tear and tensile strength are maximized at the same time is discussed. Such a design problem is typically a MONLP (Multi Objective Non Linear Program), which in the most general case can be written as follows:

$$\begin{aligned} &\max \mathbf{J}(\mathbf{x}, \mathbf{p}) \\ &\text{subject to} \begin{cases} \mathbf{g}(\mathbf{x}, \mathbf{p}) \le \mathbf{0} \\ \mathbf{h}(\mathbf{x}, \mathbf{p}) = \mathbf{0} \end{cases} \\ &\mathbf{J} = [J_1\, J_2 \ldots J_m]^T \\ &\mathbf{x} = [x_1\, x_2 \ldots x_n]^T \\ &\mathbf{g} = \left[g_1\, g_2 \cdots g_{m_g}\right]^T \\ &\mathbf{h} = [h_1\, h_2 \ldots h_{m_h}]^T \end{aligned} \tag{18}$$

Where $\mathbf{J} = [J_1\ J_2 \ldots J_m]^T$ is an objective function vector of length m, $\mathbf{x}$ is a design vector, $\mathbf{p}$ is a vector of fixed parameters, $\mathbf{g}$ and $\mathbf{h}$ are inequality and equality constraints vectors respectively.

The most popular way of solving the MONLP problem (18), also used in this article, is to reduce it to a scalar problem in the form:

$$\max \hat{J} = \sum_{i=1}^{m} \alpha_i J_i / sf_i \tag{19}$$

Where $\hat{J}$ is an aggregated weighted sum of the individual objective functions and sf_i and α_i are the scale factor and weight of the $i - th$ objective, respectively. Typically weights are chosen such that $\sum_{i=1}^{m} \alpha_i = 1$ with $\alpha_i \ge 0$.

For the case at hand we assume $\alpha_1 = \alpha$ and $\alpha_2 = 1 - \alpha$ with $\alpha \in [0,1]$, i.e., problem (19) becomes:

$$\max \hat{J} = \frac{\alpha J_1(\mathbf{x})}{sf_1} + (1-\alpha)\frac{J_2(\mathbf{x})}{sf_2} \tag{20}$$

Furthermore, to handle a well scaled problem, we choose scale factors sf_i such that $sf_i = \max J_i$. In this way, the scalar objective function $\hat{J}$ is nondimensional assuming values from 0 to 1:

$$\max \hat{J} = \frac{\alpha \sigma_t(T_s, t)}{\max\{\sigma_t(C/C_0)\}} + (1-\alpha)\frac{F_t(T_s, t)}{\max\{F_t(C/C_0)\}} \tag{21}$$

Where all the symbols have been already introduced.

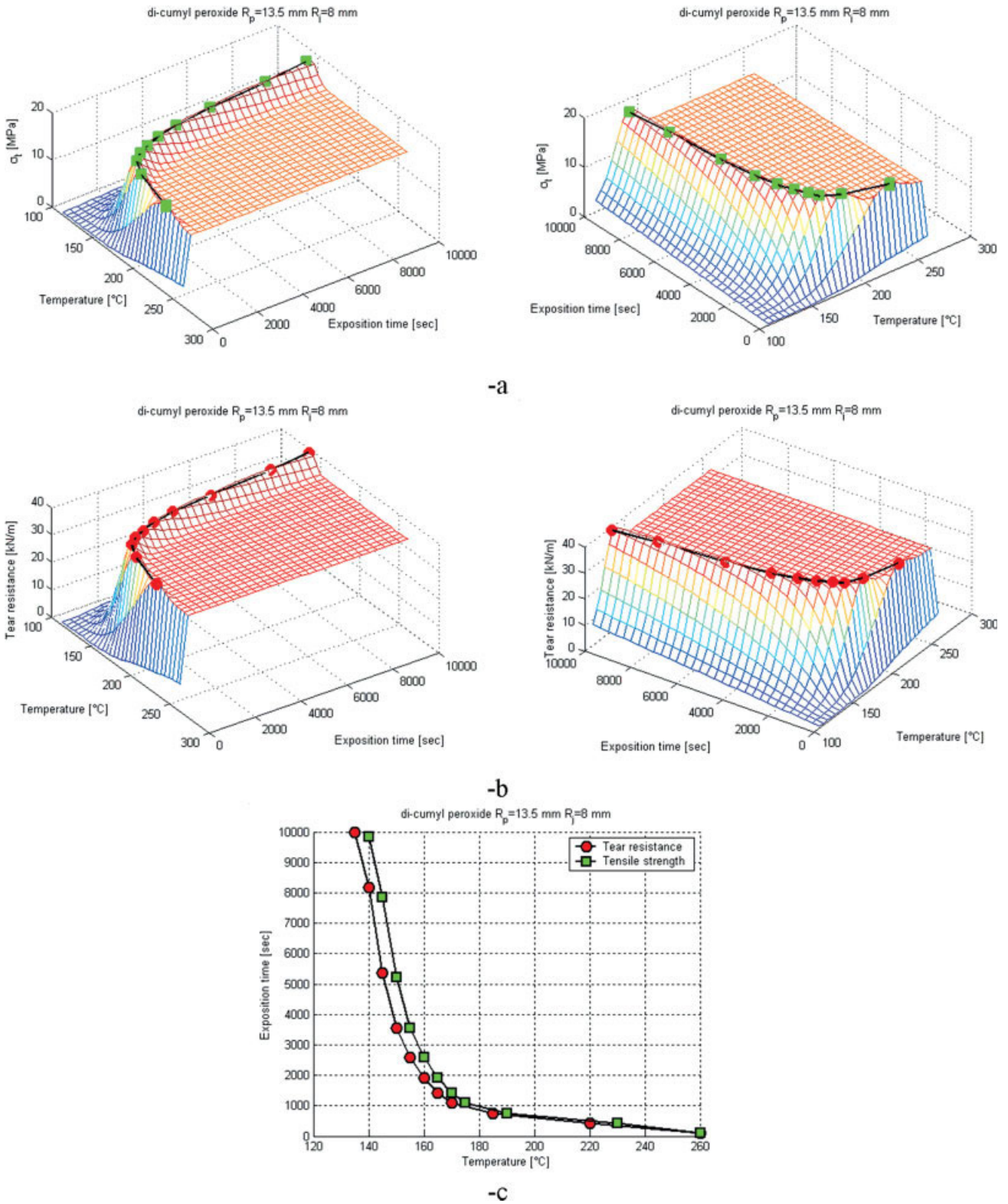

Figure 15 Di-cumyl peroxide, medium voltage cables (red circles and green squares represent GA optimization points). (a) exposition time-temperature-tensile strength surfaces. (b) exposition time-temperature-tear resistance surfaces. (c) optimal tear resistance/tensile strength exposition time-temperature curves. Optimal curing time is obtained multiplying by 1/3 exposition time. [Color figure can be viewed in the online issue, which is available at www.interscience.wiley.com.]

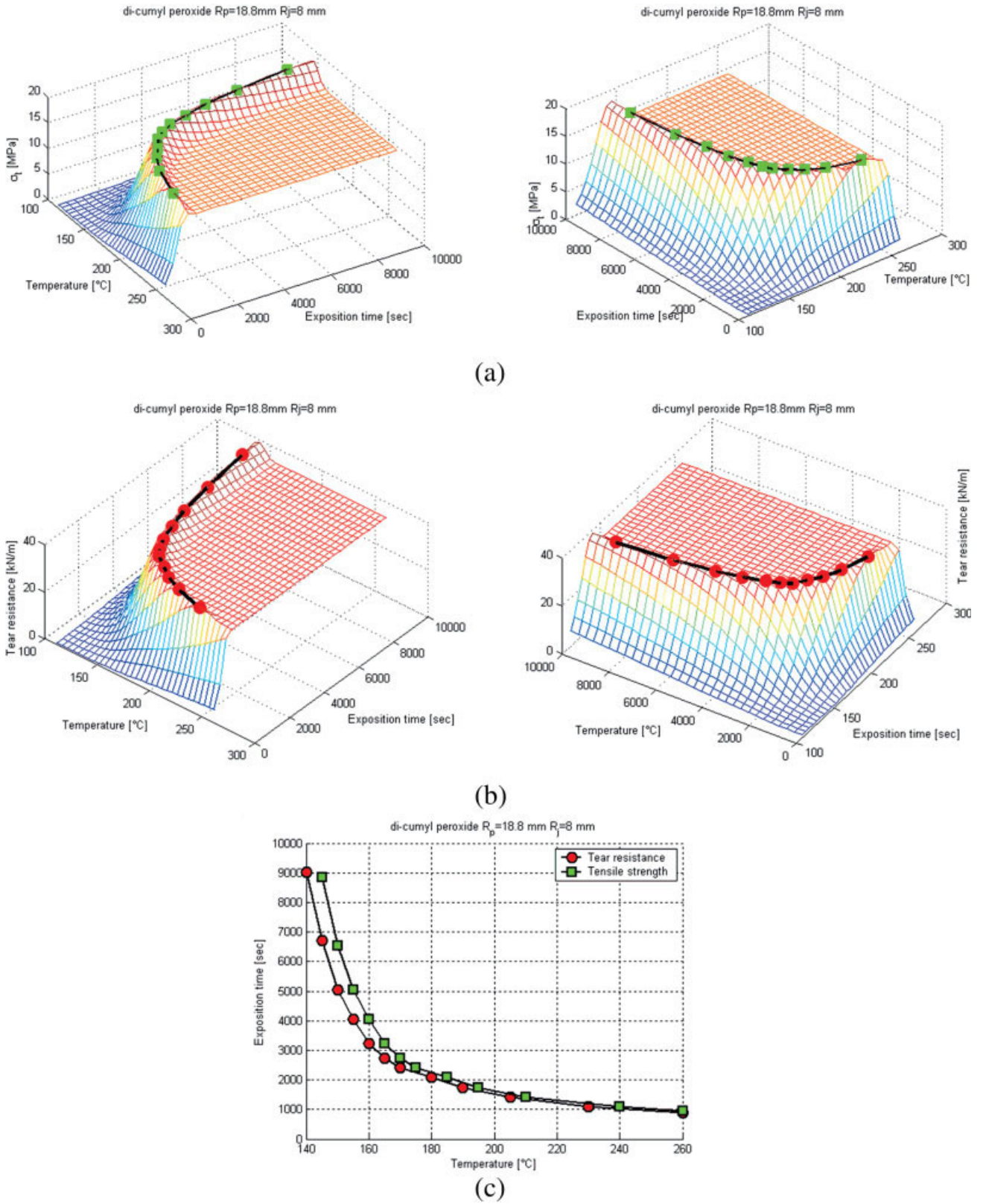

Figure 16 Di-cumyl peroxide, high voltage cables (red circles and green squares represent GA optimization points). (a) exposition time-temperature-tensile strength surfaces. (b) exposition time-temperature-tear resistance surfaces. (c) optimal tear resistance/tensile strength exposition time-temperature curves. Optimal curing time is obtained multiplying by 1/3 exposition time. [Color figure can be viewed in the online issue, which is available at www.interscience.wiley.com.]

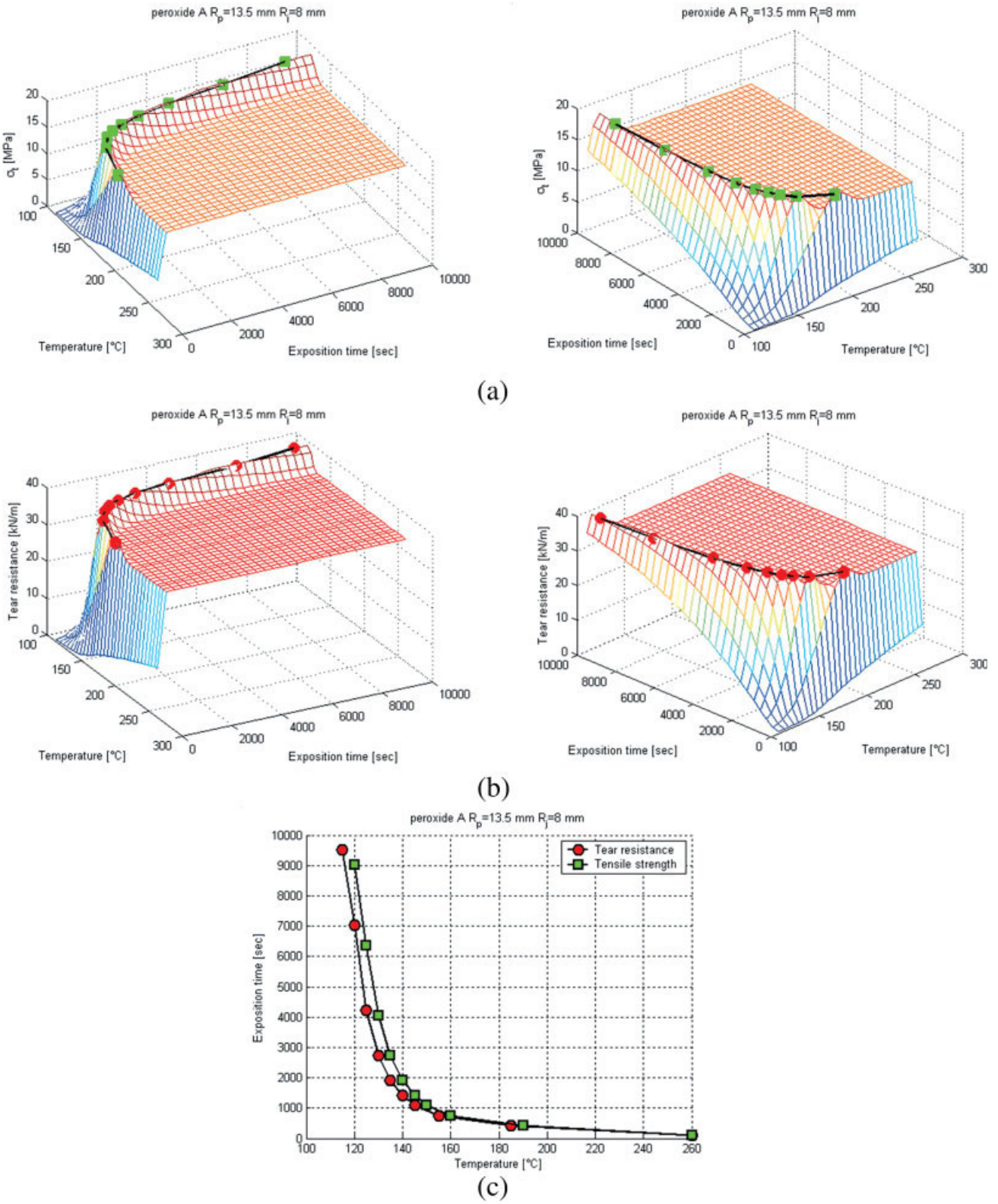

Figure 17 Peroxide A, medium voltage cables (red circles and green squares represent GA optimization points). (a) exposition time-temperature-tensile strength surfaces. (b) exposition time-temperature-tear resistance surfaces. (c) optimal tear resistance/tensile strength exposition time-temperature curves. Optimal curing time is obtained multiplying by 1/3 exposition time. [Color figure can be viewed in the online issue, which is available at www.interscience.wiley.com.]

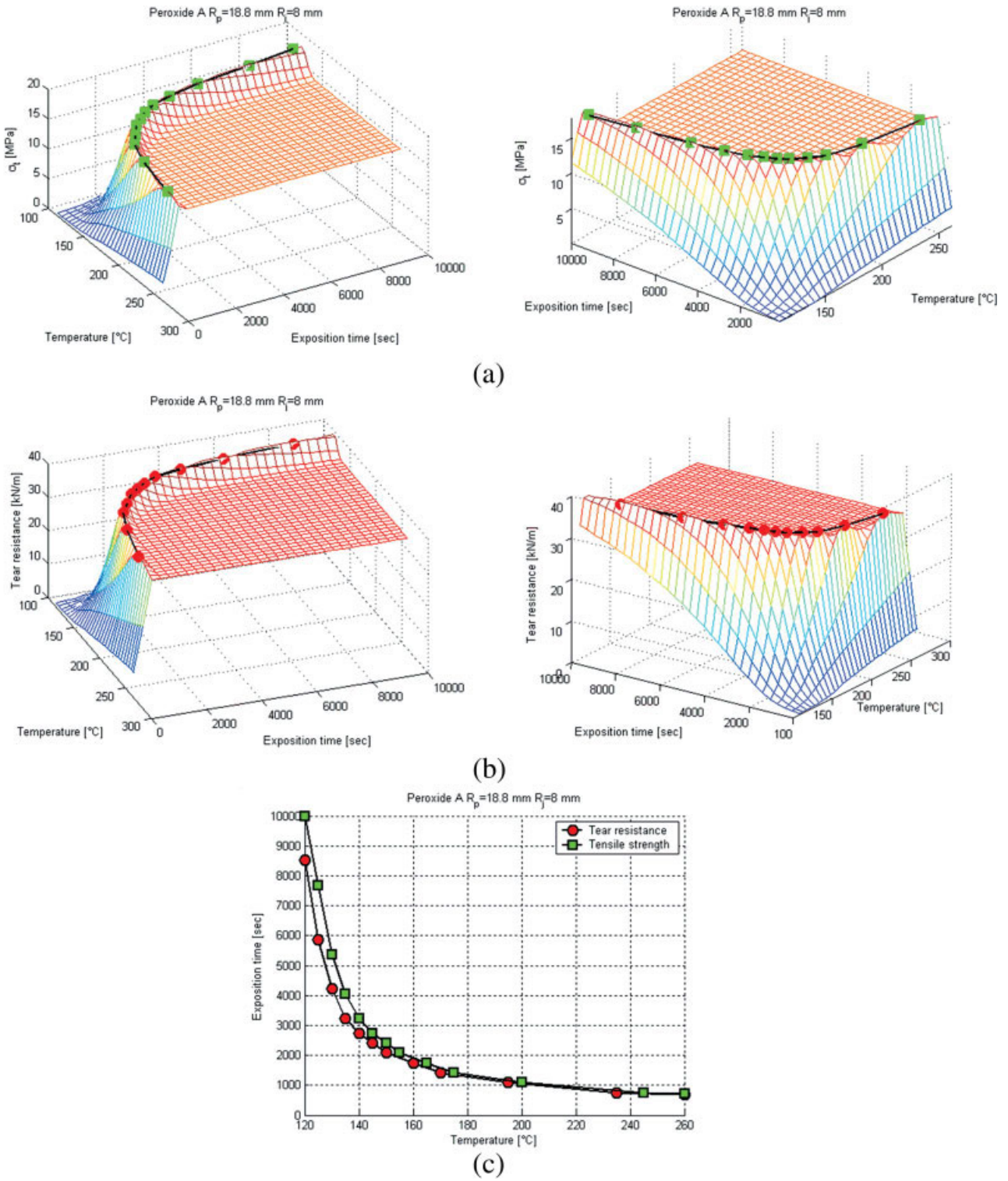

Figure 18 Peroxide A, high voltage cables (red circles and green squares represent GA optimization points). (a) exposition time-temperature-tensile strength surfaces. (b) exposition time-temperature-tear resistance surfaces. (c) optimal tear resistance/tensile strength exposition time-temperature curves. Optimal curing time is obtained multiplying by 1/3 exposition time. [Color figure can be viewed in the online issue, which is available at www.interscience.wiley.com.]

To obtain Pareto frontiers in the $J_1 - J_2$ space, for the sake of simplicity we assume alternatively one of the input variables (nitrogen temperature T_s or exposition time t) fixed. With this simplification, problem (18) reduces to a scalar nonlinear optimization problem with objective function not analytically known. To circumvent typical problems related to the weighted sum method, as for instance the

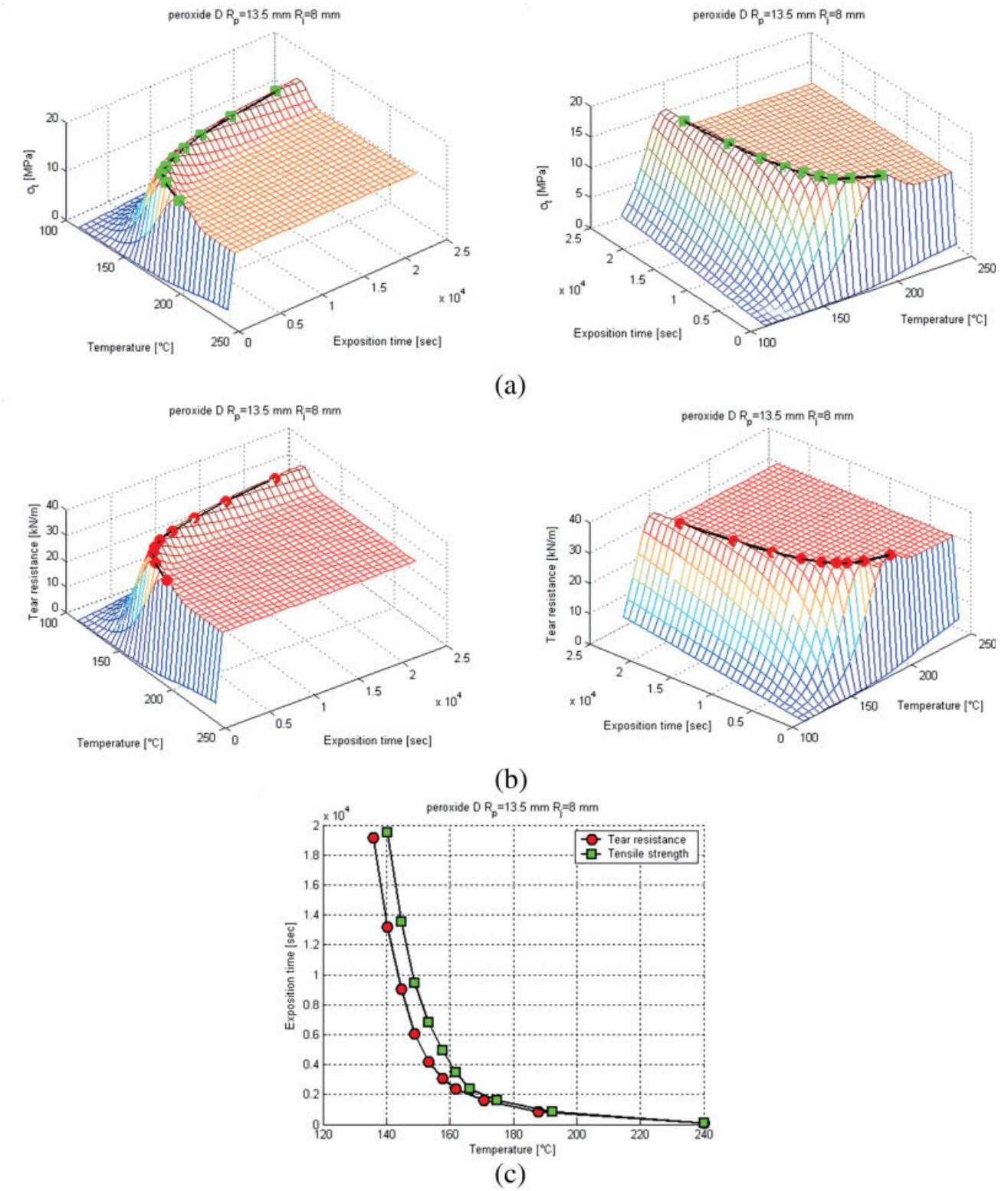

Figure 19 Peroxide D, medium voltage cables (red circles and green squares represent GA optimization points). (a) exposition time-temperature-tensile strength surfaces. (b) exposition time-temperature-tear resistance surfaces. (c) optimal tear resistance/tensile strength exposition time-temperature curves. Optimal curing time is obtained multiplying by 1/3 exposition time. [Color figure can be viewed in the online issue, which is available at www.interscience.wiley.com.]

determination of optimal points with a strongly irregular step on the Pareto frontier, here the adaptive weighted sum method proposed in Ref. 10 is used. Such method permits an evaluation of Pareto fronts with a regular step (the reader is referred to Ref. 10 for the details of the algorithm used).

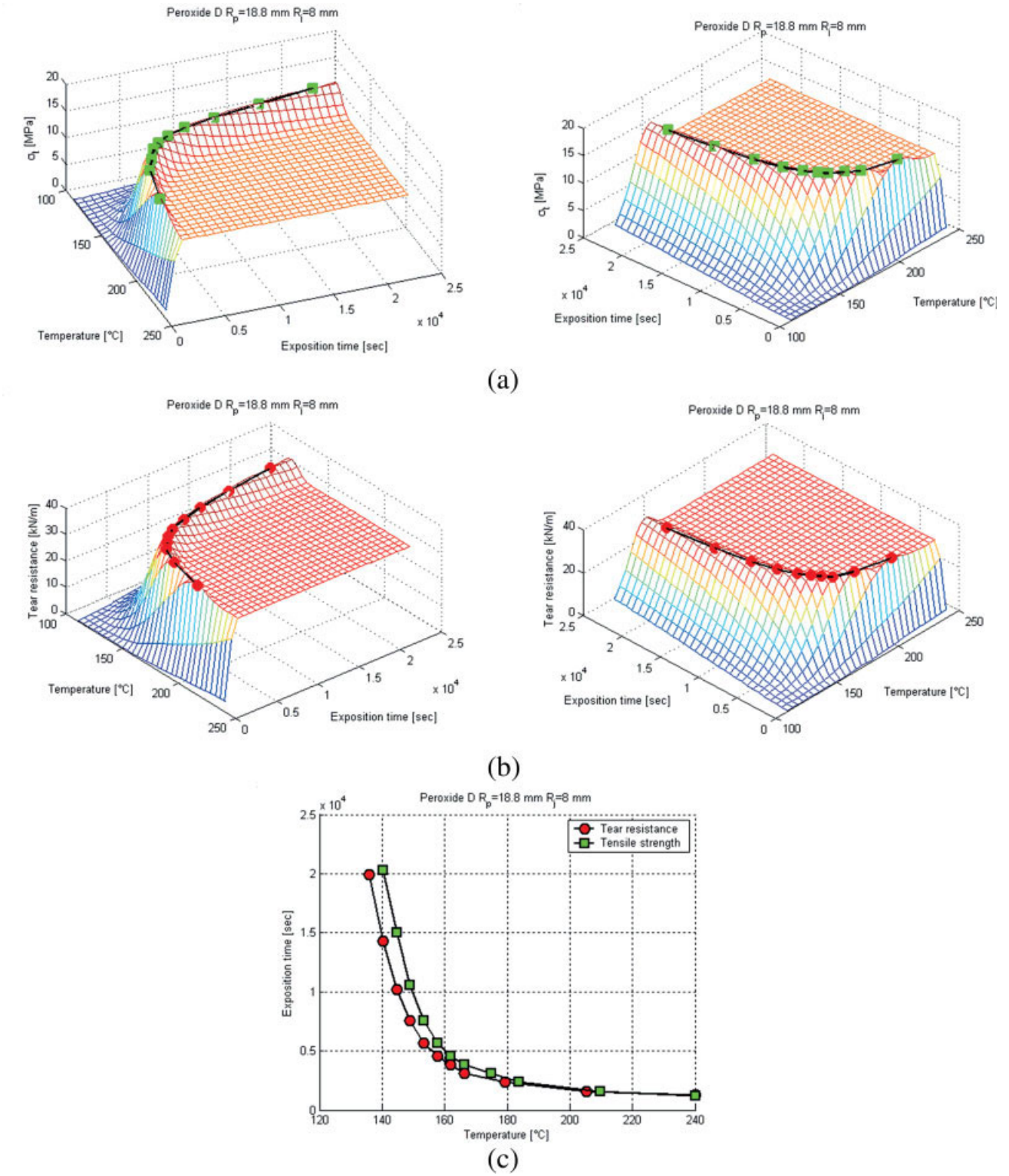

Figure 20 Peroxide D, high voltage cables (red circles and green squares represent GA optimization points). (a) exposition time-temperature-tensile strength surfaces. (b) exposition time-temperature-tear resistance surfaces. (c) optimal tear resistance/tensile strength exposition time-temperature curves. Optimal curing time is obtained multiplying by 1/3 exposition time. [Color figure can be viewed in the online issue, which is available at www.interscience.wiley.com.]

In Figure 23(a), Pareto frontier obtained solving problem (21) with the GA approach proposed is reported for an high voltage cable with di-cumyl peroxide and assuming T_s equal to 145°C. The same frontier is depicted in Figure 23(b) when t = 5000 sec and T_s is variable. Red circles

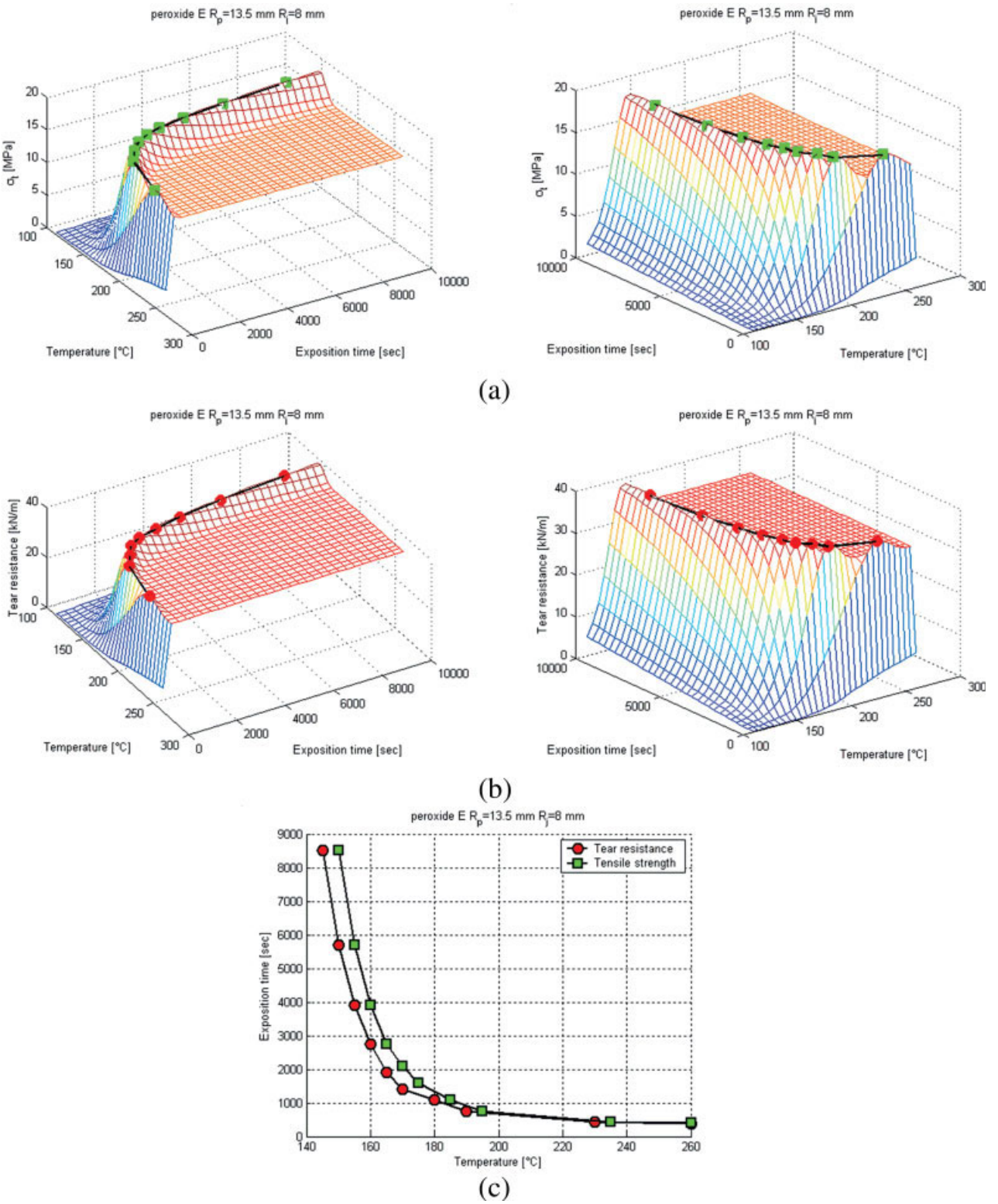

Figure 21 Peroxide E, medium voltage cables (red circles and green squares represent GA optimization points). (a) exposition time-temperature-tensile strength surfaces. (b) exposition time-temperature-tear resistance surfaces. (c) optimal tear resistance/tensile strength exposition time-temperature curves. Optimal curing time is obtained multiplying by 1/3 exposition time. [Color figure can be viewed in the online issue, which is available at www.interscience.wiley.com.]

represent GA optimization points. The convexity and the nonlinearity of both the Pareto frontiers is worth noting. On the other hand in Figure 23(c–e), σ_t and F_t optimal curves (intended as optimal weighted sum values) are depicted as a function of t or T_s.

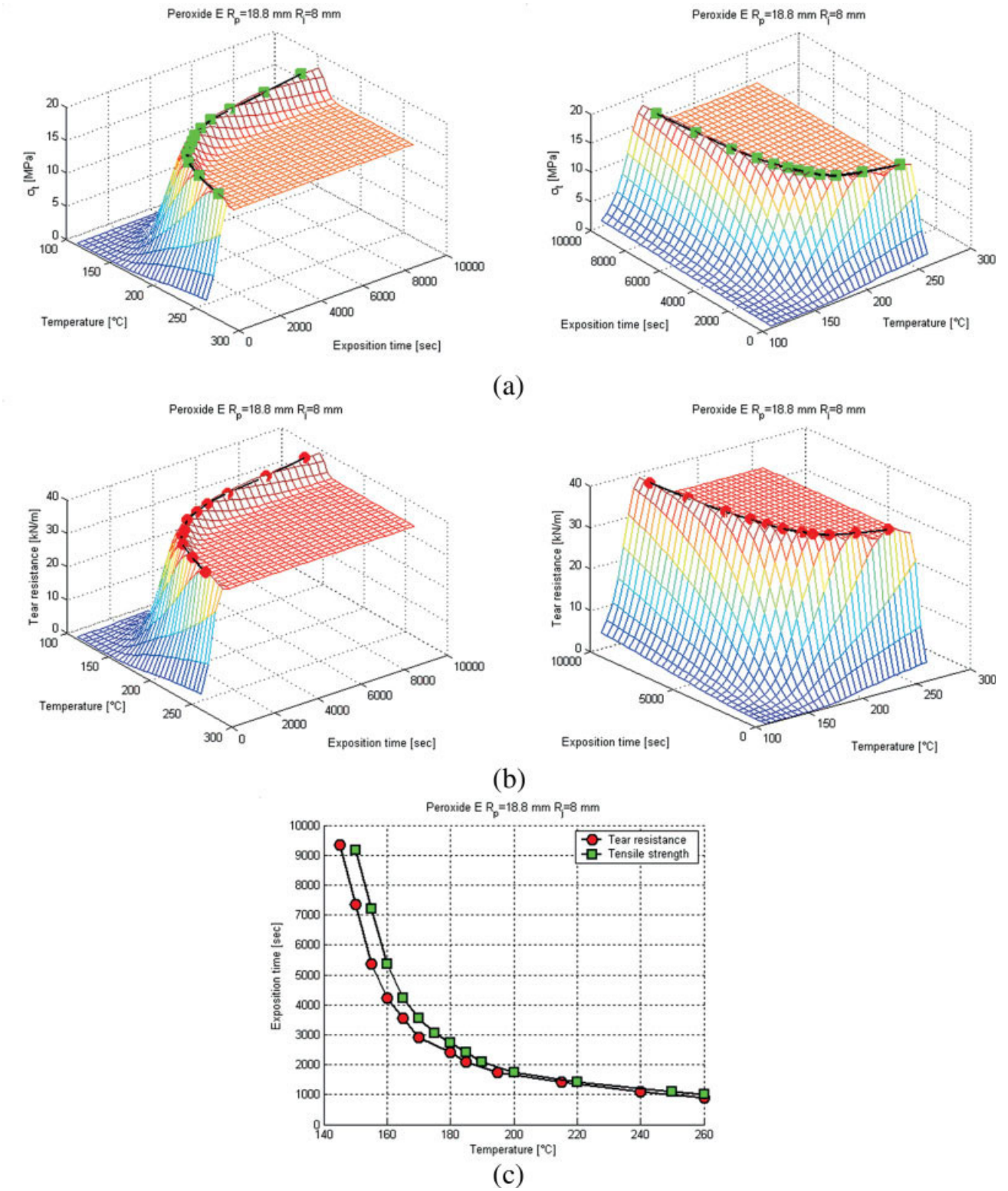

Figure 22 Peroxide E, high voltage cables (red circles and green squares represent GA optimization points). (a) exposition time-temperature-tensile strength surfaces. (b) exposition time-temperature-tear resistance surfaces. (c) optimal tear resistance/tensile strength exposition time-temperature curves. Optimal curing time is obtained multiplying by 1/3 exposition time. [Color figure can be viewed in the online issue, which is available at www.interscience.wiley.com.]

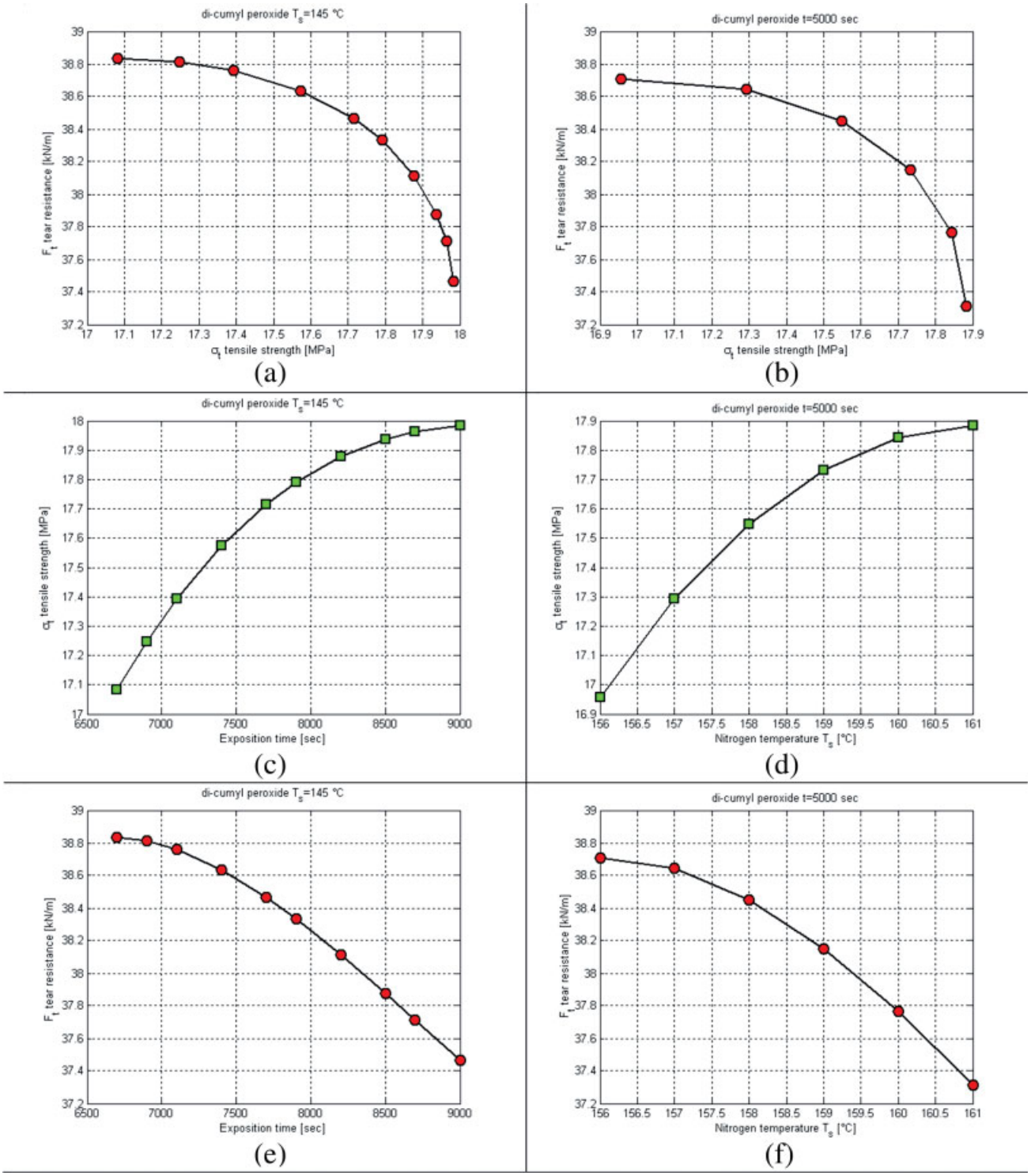

Figure 23 Di-cumyl peroxide, high voltage cables (red circles and green squares represent GA optimization points). (a) Pareto frontier, plane $\sigma_t - F_t$ at $T_s = 145°C$. (b) Pareto frontier, plane $\sigma_t - F_t$ at $t = 5000$ s. (c) $\sigma_t - t$ optimal curve, $T_s = 145°C$. (d) $\sigma_t - t$ optimal curve, $t = 5000$ s. (e) $F_t - t$ optimal curve, $T_s = 145°C$. (f) $F_t - t$ optimal curve, $t = 5000$ s. [Color figure can be viewed in the online issue, which is available at www.interscience.wiley.com.]

Despite the relatively low variability of output parameters (less that 10% both for tear resistance and tensile strength, see Fig. 23), the approach proposed results particularly useful from a practical point of view when more that one output property has to be maximized.

CONCLUSIONS

A novel genetic algorithm with zooming and elitist strategy for the determination of optimal input parameters of power cables production lines has been presented. Nitrogen temperature in the heating phase (T_s) and curing time t have been assumed as independent input variables to optimize, whereas objective functions are represented by rubber mean tensile strength and tear resistance after vulcanization. Several examples of technical relevance have been reported for both medium and high voltage cables, in presence of four different peroxides used as reticulation inducers. A detailed comparison with a classic approach based on a regular subdivision of the $T_s - t$ domain demonstrates the numerical efficiency, in terms of both processing time and reliability of the optimal solution found, of the method proposed.

A final multiobjective optimization assuming as objective function the nondimensional weighted sum of tensile and tear strength has been reported.

References

1. Drake, R. E.; Labriola, J. M.; Holliday, J. J. Improving Properties of EPM and EPDM with Coagents; American Chemical Society: Chicago, IL, 1994.
2. Drake, R. E.; Labriola, J. M.; Holliday, J. J. 1,2 Polybutadiene Coagents for Improved Elastomeric Properties; American Chemical Society: Nashville, TN, 1992.
3. Shuvalov, M.; Mavrin, M.; Ovsienko, V.; Romashkin, A. J Appl Polym Sci 2003, 88, 1543.
4. Bateman, L. Ed. The Chemistry and Physics of Rubber-Like Substances; MacLaren: London, 1963.
5. Coran, A. Y. In: Science and Technology of Rubber; Frederick, R. Eirich, Ed.; Academic Press: New York, 1978; Chapter 7.
6. Morton, M. Ed. Rubber Technology, 2nd ed.; Van Nostrand Reinhold: New York, 1981.
7. Billmeier, F. W., Jr. Textbook of Polymer Science, 3rd ed.; Wiley: New York, 1984.
8. Hofmann, W. Kautschuk gummi kunststoffe 1987; Jahrganf 4.
9. Bellander, M. High pressure vulcanization. PhD thesis; Department of Polymer Technology Royal Institute of Technology: Stockholm, 1998.
10. Kim, L. Y.; de Weck, O. L. Struct Multidisc Optim 2005, 29, 149.
11. Pareto, V. Manuale di economia politica, Società Editrice Libraria: Milano, Italy, 1906. Translated in English by Schwier, AS. Manual of Political Economy, MacMillan: New York, 1971.
12. Das, I.; Dennis, J. E. Struct Optim 1997, 14, 63.
13. Gupta, R. R.; Gupta, S. K. J Appl Polym Sci 1999, 73, 729.
14. Zhou, F.; Gupta, S. K.; Ray, A. K. J Appl Polym Sci 2000, 78, 1439.
15. Lenir, V. L. Polym Eng Sci 1984, 24, 633.
16. Roberts, B. E.; Verne, S. Plast Rubber Process Appl 1984, 4, 135.
17. Seymour, D. C.; Krick, D. J Elast Plast 1979, 11, 97.
18. Italian Railways (FS, Ferrovie dello Stato). Technical specifications for medium and high voltage cables, technical report DI/TC.TE TE 159, 1999.
19. Di Giulio, E.; Ballini, G. Kautschuk gummi kunststoffe 1962, 15.
20. Liu, J.; Yu, W.; Zhao, C.; Zhou, C. Polymer 2007, 48, 2882.
21. Baldwin, F. P.; Ver Strate, G. Rubber Chem Technol 1972, 45, 709.
22. Scanlan, J.; Thomas, D. K. J. Polym Sci Part A: Gen Pap 1963, 1, 1015.
23. Trotman-Dickinson, A. F. J Chem Educ 1969, 46, 396.
24. Encyclopaedia of Polymer Science and Technology; In Plastics, Resins, Rubbers, Fibers; Mark, H. F., Gaylord, N. G., Bikales, N. M., Eds.; Wiley: New York, 1966; Vol. 4, p 332.
25. Loan, L. D. Rubber Chem Technol 1967, 40, 149.
26. Endstra, W. C. Kautschuk gummi kunststoffe 1979, 32, 756.
27. Schwarr, R. H.; Chien, C. H. Ethylene-Propylene co and ter polymer rubber. Report 4b, Stanford Research Institute: Menlo Park, CA, 1981.
28. Kosar, V.; Gomzi, Z. Theromochim acta 2007, 457, 70.
29. ASTM D412. Standard test methods for vulcanized rubber and thermoplastic elastomers-tension.
30. ASTM D624-86. Standard test method for tear strength of conventional vulcanized rubber and thermoplastic elastomers.
31. Matlab User's Guide 2007. Available at: http://www.mathworks.com/products/matlab/ (accessed March 2007).
32. Worzakowska, M. Polymer 2007, 48, 1148.
33. Skeel, R. D.; Berzins, M. SIAM J Sci Stat Comput 1990, 11, 1.
34. Farlow, S. J. Partial Differential Equations for Scientists and Engineers; Wiley: New York, 1982.
35. Schisser, W. E. The Numerical Method of Lines: Integration and Partial Differential Equations; Academic press: San Diego CA, 1991.
36. Goldberg, D. E. Genetic Algorithms in Search, Optimization and Machine Learning; Addison Wesley Publishing Company: MA, 1989.
37. Holstien, R. B. Artificial genetic adaptation in computer control systems. Ph.D. Thesis, Department of Computer and Communication Sciences, University of Michigan, Ann Arbor, 1971.
38. Haupt, R. L.; Haupt, S. E. Practical Genetic Algorithms; Wiley: New Jersey, 2004.
39. Kwon, Y.-D.; Kwon, S.-B.; Jin, S.-B.; Kim, J.-Y. Comput Struct 2003, 81, 1715.
40. Milani, G.; Milani, F. J Comput Chem 2007, 28, 2203.
41. Lee, K. S.; Geem, Z. W. Comput Struct 2004, 82, 781.